

## INFORMATION TO USERS

This reproduction was made from a copy of a document sent to us for microfilming. While the most advanced technology has been used to photograph and reproduce this document, the quality of the reproduction is heavily dependent upon the quality of the material submitted.

The following explanation of techniques is provided to help clarify markings or notations which may appear on this reproduction.

1. The sign or "target" for pages apparently lacking from the document photographed is "Missing Page(s)". If it was possible to obtain the missing page(s) or section, they are spliced into the film along with adjacent pages. This may have necessitated cutting through an image and duplicating adjacent pages to assure complete continuity.
2. When an image on the film is obliterated with a round black mark, it is an indication of either blurred copy because of movement during exposure, duplicate copy, or copyrighted materials that should not have been filmed. For blurred pages, a good image of the page can be found in the adjacent frame. If copyrighted materials were deleted, a target note will appear listing the pages in the adjacent frame.
3. When a map, drawing or chart, etc., is part of the material being photographed, a definite method of "sectioning" the material has been followed. It is customary to begin filming at the upper left hand corner of a large sheet and to continue from left to right in equal sections with small overlaps. If necessary, sectioning is continued again—beginning below the first row and continuing on until complete.
4. For illustrations that cannot be satisfactorily reproduced by xerographic means, photographic prints can be purchased at additional cost and inserted into your xerographic copy. These prints are available upon request from the Dissertations Customer Services Department.
5. Some pages in any document may have indistinct print. In all cases the best available copy has been filmed.

**University  
Microfilms  
International**

300 N. Zeeb Road  
Ann Arbor, MI 48106

8514445

**Uz, Mehmet**

**STUDIES CONCERNING TRANSPORT OF CARBON IN NIOBIUM, VANADIUM  
AND VANADIUM-TITANIUM ALLOYS**

*Iowa State University*

PH.D. 1985

**University  
Microfilms  
International**

300 N. Zeeb Road, Ann Arbor, MI 48106

**PLEASE NOTE:**

In all cases this material has been filmed in the best possible way from the available copy. Problems encountered with this document have been identified here with a check mark .

1. Glossy photographs or pages \_\_\_\_\_
2. Colored illustrations, paper or print \_\_\_\_\_
3. Photographs with dark background \_\_\_\_\_
4. Illustrations are poor copy \_\_\_\_\_
5. Pages with black marks, not original copy \_\_\_\_\_
6. Print shows through as there is text on both sides of page \_\_\_\_\_
7. Indistinct, broken or small print on several pages  \_\_\_\_\_
8. Print exceeds margin requirements \_\_\_\_\_
9. Tightly bound copy with print lost in spine \_\_\_\_\_
10. Computer printout pages with indistinct print \_\_\_\_\_
11. Page(s) \_\_\_\_\_ lacking when material received, and not available from school or author.
12. Page(s) \_\_\_\_\_ seem to be missing in numbering only as text follows.
13. Two pages numbered \_\_\_\_\_. Text follows.
14. Curling and wrinkled pages \_\_\_\_\_
15. Dissertation contains pages with print at a slant, filmed as received \_\_\_\_\_
16. Other \_\_\_\_\_  
\_\_\_\_\_  
\_\_\_\_\_

University  
Microfilms  
International

**Studies concerning transport of carbon in niobium,  
vanadium and vanadium-titanium alloys**

by

**Mehmet Uz**

**A Dissertation Submitted to the  
Graduate Faculty in Partial Fulfillment of the  
Requirements for the Degree of  
DOCTOR OF PHILOSOPHY**

**Department: Materials Science and Engineering  
Major: Metallurgy**

**Approved:**

Signature was redacted for privacy.

**In Charge of Major Work**

Signature was redacted for privacy.

**For the Major Department**

Signature was redacted for privacy.

**For the Graduate College**

**Iowa State University  
Ames, Iowa**

**1985**

## TABLE OF CONTENTS

	Page
GENERAL INTRODUCTION	1
Explanation of Thesis Format	6
REFERENCES CITED	7
SECTION I. THERMOTRANSPORT AND DIFFUSION OF CARBON IN VANADIUM AND VANADIUM-TITANIUM ALLOYS	9
INTRODUCTION	10
THEORETICAL	12
EXPERIMENTAL	19
Materials and Apparatus	19
Thermotransport	19
Diffusion	21
Procedures	23
Thermotransport	23
Diffusion	25
RESULTS	27
Thermotransport	27
Diffusion	31
DISCUSSION OF RESULTS	38
CONCLUSIONS	46
REFERENCES CITED	47
SECTION II. THERMOTRANSPORT OF CARBON IN TWO-PHASE VANADIUM-CARBON AND NIOBIUM-CARBON ALLOYS	50
INTRODUCTION	51

THEORETICAL	53
EXPERIMENTAL	57
Materials and Apparatus	57
Procedure	58
Data acquisition	58
Calculation of concentration profiles	60
The role of second phase particles	63
RESULTS	64
Temperature Profiles	64
Carbon Mass Transport in Vanadium	64
Carbon Mass Transport in Niobium	75
Role of Second Phase Particles	81
DISCUSSION OF RESULTS	83
The Cross-Sectional Area Effect	83
Calculated and Experimental Concentration Profiles	88
$Q_{app}^*$ Versus $Q^*$	93
The Role of the Second Phase Particles	94
Solid Solubility of Carbon in Vanadium	96
CONCLUSIONS	99
REFERENCES CITED	101
APPENDIX	103
ACKNOWLEDGMENTS	109

## GENERAL INTRODUCTION

As early as the second half of the 19th century, it was known that a temperature gradient causes a redistribution of the constituent species in a homogeneous system of gases, liquids or solids. This effect was observed by Ludwig [1] in an aqueous solution of sodium sulfate, and by Soret [2-5] in various electrolyte solutions, and has since been called the Ludwig-Soret, or Soret effect. Numerous studies concerning the Soret effect in liquids [6], gases [7], and some ionic solids [8-11] have been reported in the early part of the 20th century. However, studies in solids have mostly been carried out during the last 30 years, for which case the phenomenon is called thermotransport, also referred to as thermal migration, and sometimes as thermal diffusion.

Thermotransport is a mass transport phenomenon that occurs due to a temperature gradient induced upon a solid solution alloy, and results in the development of concentration gradients as a consequence of the migration of the mobile components toward either the hot or colder regions. It may cause significant changes in the mechanical and/or physical properties of the materials involved [12]. Furthermore, in a multiphase material under a temperature gradient, the magnitude and/or direction of the transport of a solute is affected due to the presence of second phase particles, as reported for carbon in  $\alpha$ -iron [13] and Fe-Ni alloys [14], and hydrogen in zircaloy [15]. Consequently, a redistribution of second phase particles takes place which can further

alter the properties of the material.

Most engineering alloys used at elevated temperatures are multicomponent, and often multiphase. They are subjected to increasingly higher temperatures (hence, temperature gradients) for higher thermal efficiency. Therefore, studies concerning thermotransport in metals, and the effects of second phase particles on the phenomenon, are of technological interest.

The theory of thermotransport is not yet completely developed, although its phenomenological aspects are rather well understood. The macroscopic equation governing thermotransport is derived from the thermodynamics of irreversible processes [16-18]. It contains the characteristic parameter of thermotransport,  $Q^*$ , which is called the heat of transport. For the case of one-phase materials, the sign and magnitude of  $Q^*$  represents the direction and magnitude of thermotransport, with a negative sign indicating mass transport toward the hotter region of the specimen. On the other hand, when the solute concentration exceeds the solubility limit, such that it forms second phase particles with the matrix atoms, the sample is herein referred to as being in the two-phase condition. In this case, the direction and magnitude of net mass transport is dictated by the sign and magnitude of the quantity  $(Q^* + \Delta\bar{H})$ , where  $\Delta\bar{H}$  is the partial molar enthalpy of solution for the solute concerned.

The atomistic aspects of thermotransport are not thoroughly established. There is not complete agreement on the nature of the driving forces in thermotransport, i.e. the contributions to  $Q^*$ . In

general, the heat of transport is considered to consist of three contributions, namely, an intrinsic contribution,  $Q_{in}^*$ , and contributions from the interaction of the moving atoms with the phonons,  $Q_{ph}^*$ , and the charge carriers,  $Q_{el}^*$ .

The intrinsic part, which is a positive contribution, arises from the differences in the atomic jump frequencies on either side of a plane perpendicular to the temperature gradient. Wirtz [19] and Wirtz and Hiby [20] were the first to develop an atomistic theory for thermotransport, which is known as the Wirtz model. They suggested that the heat of transport would be the difference between the migration energy carried by the moving atom, and the energy necessary to prepare the receiving site. According to the Wirtz model, the magnitude of  $Q^*$  should be less than, or equal to the activation energy for diffusion. However, this does not hold true for all the systems studied; for example, for carbon in  $\alpha$ -Fe,  $\Delta\bar{H}$  is about 63 kJ/mol [21], while  $Q^*$  is approximately -104 kJ/mol [22]. The model has been discussed in some detail by various authors [12, 23-26], and Huntington [26] feels that it should be valid if one considers only the intrinsic part of  $Q^*$ . Furthermore, in a recent study concerning thermotransport of hydrogen and deuterium in vanadium and its alloys [27], Peterson and Smith have considered the intrinsic contribution to be equivalent to the activation energy for diffusion.

The phonon contribution has been discussed by Fiks [28], Schottky [29], Huntington [26, 30], and more recently by Sorbello [31].

It is considered to be due to the scattering of phonons by the atoms; however, the transfer of momentum by the phonons to an atom is questioned by Huntington [26]. This contribution is believed to be negligible in metals, since electrons, rather than phonons, carry all the charge and most of the heat. Furthermore, it is argued that the phonon contribution should be shielded by the electronic and intrinsic contributions [12, 30, 31].

The electronic contribution is attributed to the inelastic scattering of the charge carriers (electrons or holes) by the impurity atoms. It was first proposed by Fiks [32], then treated by Gerl [33], and extended to the multiband case by Huntington [30]. The latter divided it into the direct influence of electrons and/or holes, and the effect of the electrostatic fields (Thomson effect). Recently, Jones [34] proposed that the conduction electrons contribute to thermotransport through the driving forces due to (i) their unsymmetrical momentum distribution in a temperature gradient, (ii) the internal thermoelectric field, and (iii) the dependence of interionic forces or interaction potentials on the electron number density. This contribution can either be positive or negative, depending on whether the electrons moving in the direction of the temperature gradient or those moving in the opposite direction are more effective in driving the atoms. Huntington [30] estimated that  $Q_{el}^*$  for self-thermotransport in platinum is a large positive value, and Hehenkamp [12] calculated it to be negative for germanium in copper, and tin in silver. Furthermore,

similarities in the behavior of  $Q^*$  and thermoelectric power  $S$ , giving rise to a linear relationship between them, were reported for oxygen in tantalum upon the addition of tungsten, rhenium and nitrogen [35]. The above arguments and observations, together with the sign correlation between  $Q^*$  and the effective valence,  $Z^*$  [36], tend to support the presence of a significant electronic contribution to thermotransport in metals and alloys.

The data on thermotransport is relatively limited, and the atomistic aspects of the phenomenon are not well understood. It is not possible, at present, to experimentally determine the significance, and/or magnitudes, of  $Q_{el}^*$  or  $Q_{in}^*$  separately. However, in a given system, concurrent studies of the effects of various parameters (solute concentration, temperature, alloying additions) on  $Q^*$ , and on the characteristic parameters of related phenomena whose atomistic aspects are better known (diffusion, thermoelectric power, electrotransport), should yield valuable information. More data are necessary, however, for a better understanding of the atomistic aspects of thermotransport.

The present studies deal with the thermotransport and diffusion of carbon in vanadium, and V-Ti alloys, and the two-phase mass transport of carbon in vanadium and niobium. Here, a critical examination of the thermotransport theory and existing atomistic models is attempted, and the results of the systematic study of the effects of the second phase particles on the phenomenon are presented. The use of the ultrahigh vacuum apparatus made it possible to obtain data virtually free of any effects due to interaction with the environment, e.g. carburization

and/or decarburization, which would have led to erroneous results [36]. Furthermore, each of the studies in this manuscript is one of the relatively few investigations of its kind, i.e. mass transport in ternary, and two-phase systems under a temperature gradient.

#### Explanation of Thesis Format

This thesis has been written in the alternate format which is outlined in The Graduate College Thesis Manual. The main body of this thesis consists of two papers which are designated as Sections I and II. The paper designated as Section I has been presented at the 1984 TMS-AIME Annual Meeting, Los Angeles, California, February 28, 1984. Both papers are the sole work of Dr. O. N. Carlson and myself, and are to be submitted for publication shortly.

## REFERENCES CITED

1. C. Ludwig, Sitzber. Akad. Wiss. Wein, Math.-Naturw. Klasse 20, 539 (1856).
2. C. Soret, Arch. Sci. Phys. Nat. 3, 48 (1879).
3. C. Soret, Arch. Sci. Phys. Nat. 4, 209 (1880).
4. C. Soret, Compt. Rend. 91, 289 (1880).
5. C. Soret, Ann. Chim. Phys. 22, 293 (1881).
6. W. Jost, Diffusion in Solids, Liquids and Gases (Academic Press, New York, 1952), p. 489.
7. J. Hirschfelder, C. F. Curtiss and R. B. Bird, The Molecular Theory of Gases and Liquids (John Wiley and Sons, New York, 1954), p. 516.
8. H. Reinhold, Z. Phys. Chem. A141, 137 (1929).
9. H. Reinhold, Z. Electrochem. 35, 627 (1929).
10. H. Reinhold and R. Schulz, Z. Phys. Chem. A164, 241 (1933).
11. H. Reinhold and H. Seidel, Z. Phys. Chem. B38, 245 (1937).
12. T. Hehenkamp, in Electro- and Thermo-transport in Metals and Alloys, edited by R. E. Hummel and H. B. Huntington (AIME, Inc., New York, 1977), p. 68.
13. P. G. Shewmon, Trans. Met. Soc. AIME 212, 642 (1958).
14. I. C. I. Okafor, O. N. Carlson and D. M. Martin, Metall. Trans. A 13A, 1713 (1982).
15. A. Sawatzky, J. Nuc. Mater. 2, No. 4, 321 (1960).
16. I. Prigogine, Introduction to Thermodynamics of Irreversible Processes, 2nd edition (Interscience Publishers, New York, 1961).
17. S. R. DeGroot, Thermodynamics of Irreversible Processes (Interscience Publishers, New York, 1952).
18. K. G. Denbigh, The Thermodynamics of Steady State (John Wiley and Sons, Inc., New York, 1965).

19. K. Wirtz, Phys. Z. 44, 221 (1943).
20. K. Wirtz and J. W. Hiby, Phys. Z. 44, 369 (1943).
21. F. D. Richardson, AISI Trans. 175, 33 (1953).
22. L. Darken and R. Oriani, Acta Metall. 2, 84 (1954).
23. A. D. LeClaire, Phys. Rev. 93, No. 2, 344 (1954).
24. J. A. Brinkman, Phys. Rev. 93, No. 2, 345 (1954).
25. L. A. Ginifalco, Phys. Rev. 128, No. 6, 263 (1962).
26. H. B. Huntington, in Diffusion (ASM, Metals Park, Ohio, 1973), p. 155.
27. D. T. Peterson and M. F. Smith, Metall. Trans. A 13A, 821 (1982).
28. V. B. Fiks, Sov. Phys.-Sol. State (English Transl.) 3, 724 (1962).
29. G. Schottky, Phys. Stat. Sol. 8, 357 (1965).
30. H. B. Huntington, J. Phys. Chem. Sol. 29, 1641 (1968).
31. R. S. Sorbello, in Electro- and Thermo-transport in Metals and Alloys, edited by R. E. Hummel and H. B. Huntington (AIME, Inc., New York, 1977), p. 68.
32. V. B. Fiks, Sov. Phys.-Sol. State (English Transl.) 5, No. 12, 2549 (1964).
33. M. Gerl, J. Phys. Chem. Sol. 28, 725 (1967).
34. W. Jones, J. Phys. F: Met. Phys. 12, 87 (1982).
35. J. Mathuni, R. Kirchheim and E. Fromm, Acta Metall. 27, 1665 (1979).
36. O. N. Carlson, F. A. Schmidt and M. Uz, J. Less-Common Metals 79, 97 (1981).

**SECTION I. THERMOTRANSPORT AND DIFFUSION OF CARBON IN  
VANADIUM AND VANADIUM-TITANIUM ALLOYS**

## INTRODUCTION

The atoms in an initially homogeneous material undergo redistribution when subjected to a temperature gradient, and are transported toward either the hotter or colder regions of a sample, depending on the metal or alloy under investigation. This mass transport phenomenon, referred to as thermotransport or thermomigration, has been the subject of research for many years. A detailed discussion of the phenomenon, and some of its consequences, can be found in a publication by Hehenkamp [1].

Vanadium base alloys are considered as candidates for use at high temperatures [2, 3], an alternative structural material for fast breeder reactors, and the first wall material for fusion reactors [4, 5]. In all these applications, large temperature gradients will certainly exist. The V-Ti system consists of a complete series of solid solutions in the temperature range of interest [6], and the diffusivity of carbon in both vanadium [7] and titanium [8] is relatively high. Also, all of the previous thermotransport studies, with two exceptions [9, 10], were carried out in dilute binary solid solutions, and an extensive list of references of thermotransport studies has been given in a review paper by Wever [11].

Diffusion, also a mass transport phenomenon, is associated with concentration gradients, and is usually studied under isothermal, non-steady state conditions. As is the case for thermotransport, most of the diffusion studies have been carried out in binary solid

solutions, and investigations in ternary systems are quite limited. The diffusion studies in this investigation were made primarily to determine the possible correlation between the activation energy for diffusion,  $\Delta H$ , and the heat of transport,  $Q^*$ , of carbon in vanadium from a comparison of the effects of titanium additions on these parameters.

Most engineering materials are multicomponent alloys, and are constantly being subjected to higher temperatures and greater temperature gradients. Both diffusion and thermotransport often result in drastic changes in the physical and mechanical properties of the materials involved [1]; hence, a study of these phenomena in multicomponent systems should be of significant technological interest. Also, more data are necessary as a basis for a better understanding of the transport phenomena in solids. This paper deals, in particular, with the effects of titanium additions on the thermotransport and diffusion characteristics of carbon in vanadium.

## THEORETICAL

The general theory of and the driving forces in the thermotransport phenomenon have been reviewed in some detail by several authors [1, 12-22]; therefore, only a brief summary will be given in this section. That will be the case for diffusion, since its theory and mechanisms have been the subject of numerous books and papers.

In this study, the V-Ti-C system is treated as a binary one, since the mobilities of vanadium and titanium are negligible in comparison to that of carbon, i.e., the V-Ti matrix acts as a stationary frame of reference for the migrating carbon atoms. This treatment is quite valid, since in a V-10 at.% Ti alloy, at 1373 K for example, the diffusion coefficient of carbon as determined in the present study is of the order of  $10^{-7}$  cm<sup>2</sup>/sec, whereas that of titanium and vanadium is of the order of about  $10^{-12}$  cm<sup>2</sup>/sec [23].

Phenomenologically, the macroscopic equations governing thermotransport can be derived using the principles of irreversible thermodynamics [24, 25]. The flux of a mobile specie *i* in an ideal solid solution alloy under a one-dimensional temperature gradient, in the absence of any other external fields, can be expressed as

$$J_i = - \frac{D_i C_i}{RT} \left[ \frac{RT}{C_i} \frac{dC_i}{dX} + \frac{Q_i^*}{T} \frac{dT}{dX} \right] , \quad (1)$$

where *R* is the gas constant, *T* is the absolute temperature, *D<sub>i</sub>* and *C<sub>i</sub>* are the diffusion coefficient and concentration of specie *i*,

respectively, and  $Q_1^*$  is its heat of transport. The first and second terms within the brackets of Equation (1) represent the forces due to the concentration and temperature gradients, respectively. Most thermotransport studies are carried out at or near steady-state conditions, i.e. as  $J_1 \rightarrow 0$ ; thus, Equation (1) becomes

$$d \ln C = \frac{Q_1^*}{R} d\left(\frac{1}{T}\right) . \quad (2)$$

The direction and magnitude of thermotransport are represented by the sign and magnitude of  $Q_1^*$ , with a negative value indicating solute migration toward the hotter regions of the specimen.

The Grube solution [26] for two semi-infinite rods of different compositions joined together was used in obtaining the diffusion coefficients. For one-dimensional diffusion [27, 28], it is expressed as

$$C_x = C_1 + \frac{C_2 - C_1}{2} \left[ 1 - \operatorname{erf} \frac{X}{\sqrt{4Dt}} \right], \quad (3)$$

where  $C_x$  is the solute concentration at a distance  $X$  along the rod in the direction of the concentration gradient after time  $t$  at the annealing temperature,  $C_2$  and  $C_1$  are the high and low concentrations, respectively, and  $D$  is the diffusion coefficient. In obtaining Equation (3), it was assumed that (i) the concentrations at the ends of the diffusion couple do not change during the heating period, (ii) the amount of solute depleted from the high-concentration half of

the diffusion couple equals that gained by its low concentration half, and (iii) at the beginning of the diffusion anneal, the concentration at the weld interface can be defined by a mean concentration as

$$C_M = \frac{C_1 + C_2}{2} \quad (4)$$

and stays constant throughout. Combining Equations (3) and (4), one obtains

$$\frac{C_x - C_M}{C_2 - C_M} = - \operatorname{erf} \frac{x}{\sqrt{4Dt}} \quad (5)$$

The theory of thermotransport is not as well developed as that of diffusion. Its phenomenological aspects are rather well understood, but that is not true for the atomistic interpretation of the phenomenon. There is not complete agreement on the nature of the driving forces in thermotransport, i.e. what constitutes the heat of transport. At present, an examination of thermotransport theory indicates that the heat of transport can be considered as the sum of three contributions, i.e.

$$Q^* = Q_{in}^* + Q_{el}^* + Q_{ph}^* \quad (6)$$

where  $Q_{in}^*$  is the intrinsic contribution, and  $Q_{el}^*$  and  $Q_{ph}^*$  are contributions due to interaction of electrons and phonons with the moving atoms.

The phonon scattering contribution is believed to be negligible in thermotransport in metals, since electrons and/or holes, rather than phonons, carry the charge and most of the heat in metals. In his analysis of this contribution, Sorbello [19] shows that phonons should exert a force on an interstitial atom in the direction of phonon current (opposite to the temperature gradient) if the impurity is heavier than the matrix atoms, and in the opposite direction if it is lighter. Carbon, according to Sorbello's analysis, would have migrated toward the colder regions of a thermotransport sample if the phonon scattering contribution were dominant. Furthermore, the possibility that phonons can transfer momentum is questioned by Huntington [16], and this contribution is believed to be shielded by intrinsic and electronic contributions.

The intrinsic contribution is considered to be due to the temperature-related differences in the atomic jump frequencies on either side of a plane perpendicular to the temperature gradient. Since there will be a larger number of atoms on the hotter side of that plane with enough energy to make a jump to its colder side than vice versa, the intrinsic contribution should always be positive, i.e. cause atoms to migrate from the hot to colder end of the specimen. There is no well-accepted atomistic models representing this contribution, but it has been suggested [9] that it should be equivalent to the activation energy for diffusion, and may be the dominant contribution when  $Q^*$  is positive.

The electronic contribution to  $Q^*$  is attributed to the interaction between the charge carriers (electrons and/or holes) and the impurity atoms, and has been discussed in some detail by several authors [1, 13, 15, 16, 19, 21]. Theoretical calculations show that this contribution is directly proportional to the effective valence,  $Z^*$ , and can be expressed as [15]

$$Q_{el}^* = \frac{\pi^2 k^2 T^2}{3E_F} \left( \frac{d \log \rho_d}{d \log E} \right) Z^* , \quad (7)$$

where  $k$  is the Boltzmann constant,  $T$  is the absolute temperature,  $\rho_d$  is the specific resistivity, and  $E_F$  and  $E$  are the Fermi and electron energies, respectively. Hehenkamp [1], using the definition of thermoelectric power, i.e.  $S = -(\pi^2 k^2 T / 3E_F) (d \log \rho_d / d \log E)$ , suggests that  $Q_{el}^*$  is also proportional to  $S$ ; hence, he expresses it as

$$Q_{el}^* = - S Z^* T . \quad (8)$$

A physical interpretation of the contribution to  $Q^*$  from the scattering of electrons by impurities can be made as follows: in a metal sample under a temperature gradient, a flux of fast (hot) electrons carrying heat down the temperature gradient should be balanced by a flux of slow (cold) electrons in the opposite direction to maintain the electrical neutrality in the specimen. The direction that a migrating impurity will be affected depends on the collision frequency, and thus,

its scattering cross-section for either type of electrons. If, as is argued by Huntington [18], the decrease of cross-section with increasing electron energy overbalances the increase in velocity, then  $Q_{el}^*$  is negative, indicating that the slower electrons will be more effective in driving the atoms up the temperature gradient. Huntington [16] believes that the correlation given by Equation (7) should hold well for simple metals with one band, and suggests that  $Q_{el}^*$  can be even larger in cases of those transition metals where electrons and holes are simultaneously operative. Also, in a metal under a temperature gradient, there will always be additional contributions from Thomson effect, and Sorbello [19] suggests that local electron polarization around a base ion might give rise to additional forces on a moving ion. Furthermore, in a recent publication, Jones [21] analyzes the electronic contribution in thermotransport, and develops a detailed theory in which he suggests that the direct influence of the conduction electrons on the thermotransport of an ion is represented by the thermal driving force on the ion. He correlates this with the contribution of the ion to thermoelectric power, which is similar to the case of electrotransport where the driving force is directly related to the contribution of the ion to the resistivity. He believes that the conduction electrons will contribute to thermotransport because of their unsymmetrical momentum distribution in a temperature gradient, internal thermoelectric field, and the dependence of interaction potential on the electron number density.

The significance of the driving forces in thermotransport, and the models developed therefrom, will be further examined in a later section.

## EXPERIMENTAL

## Materials and Apparatus

Thermotransport

The vanadium and titanium metals were obtained from the Materials Preparation Center of the Ames Laboratory in arc-melted ingot form. The total metallic impurity content, as determined by spark source mass spectrometric analysis, was less than 500 at. ppm. in vanadium, and less than 600 at. ppm. in titanium.

Vanadium was doped with  $^{14}\text{C}$ , followed by the addition of various amounts of titanium by arc melting under a partial pressure of purified argon. The V-Ti alloys contained 1.1, 2.1, 5.3, 10.5 and 20.5 at.% titanium as determined by spectrophotometric analysis. The arc-melted ingots were subsequently swaged into rods of about 0.28 cm in diameter, and then deoxidized by treatment with calcium, as described by Peterson *et al.* [29]. The carbon, nitrogen and oxygen contents of the V-Ti alloys are given in Table 1.

In studying the transport characteristics of a particular solute in metals, it is extremely important to avoid loss of the solute to, or its pickup from the environment, since these will lead to erroneous results. In an earlier study [30], the authors showed that when a Nb-C specimen is heated either in a chamber evacuated by an oil diffusion pump, or in one backfilled with a partial pressure of gettered commercial grade argon or helium gas, it undergoes carburization and/or decarburization depending on the chamber and heating times. Furthermore, it was also shown that during such thermotransport experiments, the

Table 1. Carbon, nitrogen and oxygen contents of vanadium-titanium alloys

Titanium content (at.%)	Impurity content (at.%)		
	Carbon <sup>a</sup>	Nitrogen <sup>b</sup>	Oxygen <sup>b</sup>
0.0	0.038	0.004	0.019
0.0	0.457	0.054	0.007
1.1	0.055	0.011	0.010
2.1	0.020	0.007	0.012
5.3	0.024	0.014	0.006
10.5	0.062	0.019	0.010
20.5	0.144	0.003	0.026

<sup>a</sup>Combustion chromatographic analysis.

<sup>b</sup>Vacuum fusion analysis.

sample was enriched with respect to  $^{14}\text{C}$  at the colder ends, indicating gas-phase transport of carbon from the hot to colder regions of the specimen. Such environmental effects resulted in a positive  $Q^*$  value for carbon in niobium, even though it is actually negative, as determined in an ultrahigh vacuum chamber.

The ultrahigh vacuum chamber used in that earlier study [30] was also used for the present thermotransport experiments. However, due to the relatively high vapor pressures of vanadium and titanium [31], it was necessary to heat the samples under a partial pressure of an inert gas. Hence, the ultrahigh vacuum chamber was modified by the addition of a gettering chamber, which consisted primarily of a stainless

steel tube containing molecular sieve material that is capable of adsorbing oxygen-, nitrogen- and carbon-bearing gases at liquid nitrogen temperatures. The ultrahigh vacuum and gettering chambers can be seen in Figure 1. Laboratory grade helium gas was further purified by holding it in contact with the molecular sieve material under a pressure of about  $1.5 \times 10^5$  Torr in the gettering chamber cooled with liquid nitrogen. The pressure in the main chamber was of the order of  $10^{-9}$  Torr before backfilling it with purified helium to a partial pressure of about 200 Torr.

Each specimen was approximately 1.5 cm long and 0.27 cm in diameter, and was electropolished before loading into the heating chamber. Each sample was supported between two tapered tungsten adapters screwed into water-cooled copper electrodes, as is seen from the inset of Figure 1, and was heated by internal resistance using an a.c. power source. The temperatures were measured by an optical pyrometer telescope rotating on a base equipped with a vernier scale.

### Diffusion

The high carbon sections of the diffusion samples were taken from the V-10.5 and 20.5 at.% Ti alloy rods, and the low carbon sections were obtained by solid state decarburization of these alloys by a method similar to that used for solid state deoxygenation of vanadium [32]. Each alloy rod was wrapped in a 0.01 cm thick zirconium foil and vacuum-sealed inside an outgassed tantalum tube by electron-beam welding. It was then heated at 1423 K for 24 hours in a vacuum furnace. By this method, the carbon concentration was reduced

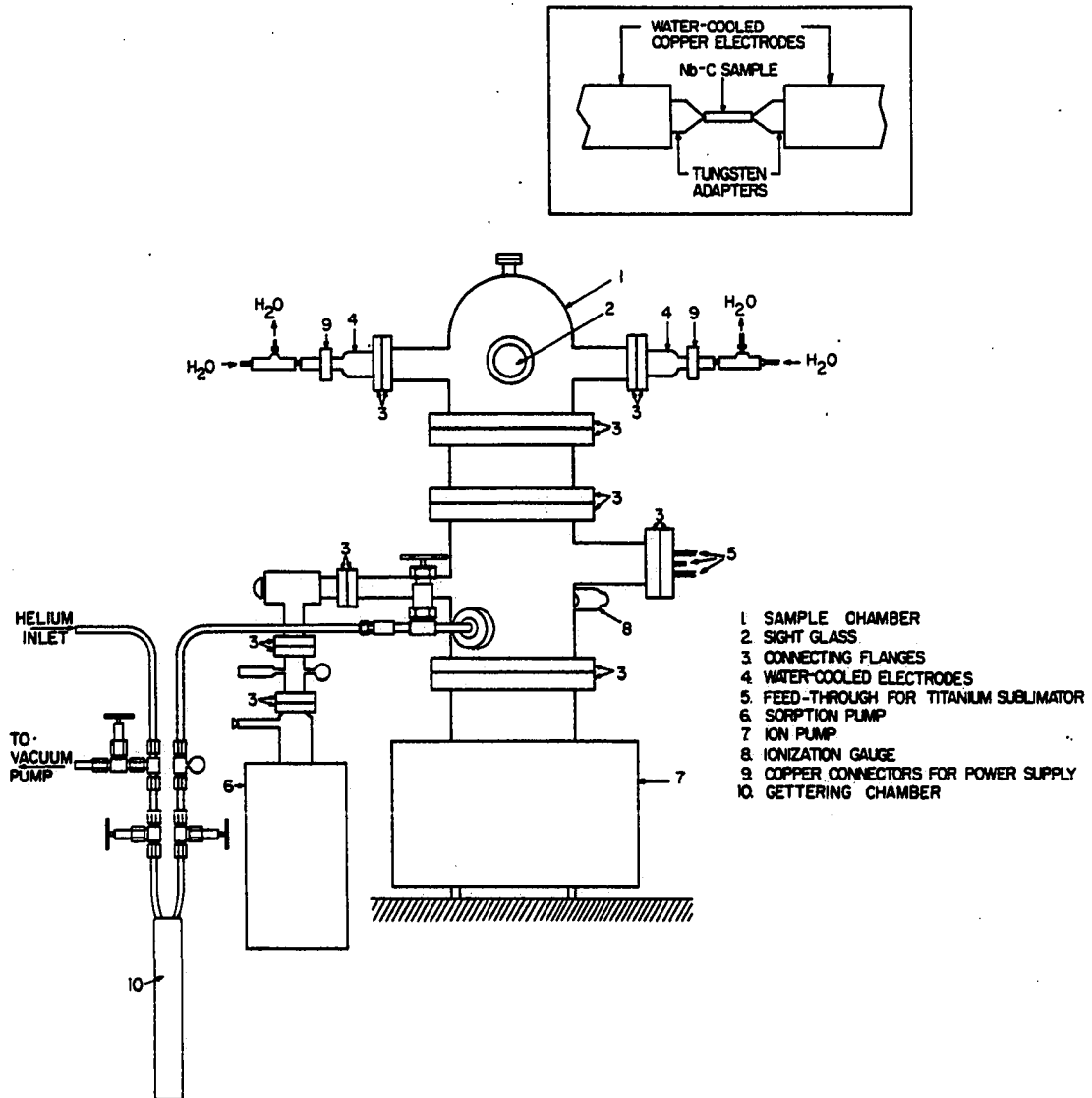


Figure 1. Ultrahigh vacuum chamber, gettering chamber, and sample arrangement (inset) for thermotransport experiments

from 615 to 200 at. ppm. in the V-10.5 at.% Ti, and from 1433 to 260 at. ppm. in the V-20.5 at.% Ti alloy.

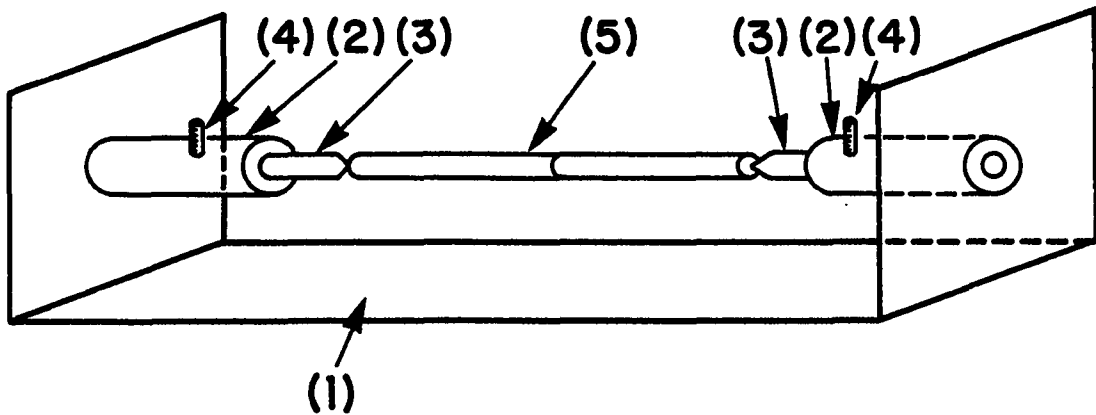
Each couple was about 2.54 cm long and 0.25 cm in diameter, and consisted of equal lengths of the high- and low-carbon rods of the same alloy butt-welded together under vacuum. It was supported between two tapered tungsten adapters mounted onto a tantalum frame, as is seen from Figure 2. The tantalum frame was then vacuum-sealed inside a tantalum tube by electron-beam welding. All the tantalum and tungsten parts were outgassed prior to use. The diffusion anneals were made in a vacuum furnace, and the temperature of the specimen was monitored using a Pt/Pt-13% Rh thermocouple and a digital voltmeter.

It should be noted from the above descriptions of the apparatuses that during both the thermotransport and diffusion experiments, the sample was only in point contact with the tungsten adapters. This, together with the high purity helium environment used for the thermotransport studies, and the very small volume of the tantalum tubes in the diffusion experiments, virtually eliminated any environmental effects during both types of experiments. This was confirmed by the excellent material balance obtained and the absence of any significant  $\beta$ -activity in the apparatuses used.

## Procedures

### Thermotransport

The general procedure for the thermotransport experiments has been described in an earlier study [30], and will only be briefly



- (1) TANTALUM FRAME
- (2) TANTALUM ADAPTER HOUSING
- (3) TUNGSTEN ADAPTERS
- (4) STAINLESS STEEL SET SCREWS
- (5) SAMPLE

Figure 2. Sample arrangement for diffusion experiments

outlined here.

The temperature profile of each sample was determined by measuring its temperature at equidistant points along its length on its surface. Each temperature was first corrected for sight glass absorption, and then for emissivity by the following equation [33]:

$$T_t = 1.083 T_s - 27.5 , \quad (9)$$

where  $T_t$  is the true temperature in  $^{\circ}\text{C}$  and  $T_s$  is the surface temperature after correction for the sight glass absorption.

The sample was cut into eight segments with a diamond saw following each run. The segments were then ground through 600 grit, and the position of each segment was identified with respect to the left end of the specimen. The carbon distribution at steady state was determined by measuring the  $\beta$ -activity of a uniform area at the ends of each segment using a gas proportional detector scaler. The heat of transport,  $Q^*$ , was obtained from the slope of a plot of  $\ln$  CPM (counts per minute) versus the reciprocal temperature (Equation 2), as determined from a linear regression analysis of the data.

### Diffusion

Each diffusion specimen was cut into 16 segments following a run, and the position of each segment was identified with respect to the high carbon end of the couple. The diffusion coefficient,  $D$ , at each annealing temperature was obtained from a plot of  $\text{erf}^{-1}[(C_x - C_M)/(C_2 - C_M)]$

versus the distance (Equation 5).

Diffusion anneals were made at 1323, 1423 and 1578 K for each alloy, and the activation energy for diffusion,  $\Delta H$ , and the pre-exponential factor,  $D_0$ , in the Arrhenius equation

$$D = D_0 \exp \left( - \frac{\Delta H}{RT} \right) \quad (10)$$

were obtained from the slope and y-intercept, respectively, of a plot of  $\ln D$  versus the reciprocal temperature.

## RESULTS

## Thermotransport

All of the V-C thermotransport specimens were in the one-phase condition at the end, as well as at the beginning of each run, according to the data of Ghaneya and Carlson [34] and Uz and Carlson [35] for the solid solubility data of carbon in vanadium and as confirmed from the metallographic examination of the samples. There was no solid solubility data available for carbon in V-Ti alloys, but metallographic examination of these samples showed that they were in the one-phase condition also.

The plots of temperature and concentration (CPM) versus distance, shown in Figure 3, for a V-1.1 at.% Ti alloy are typical of those obtained for all the thermotransport experiments in this study. A sketch of the specimen identifying the relative position of each segment is also shown in the upper part of the figure. As is seen from this figure, both the temperature and concentration profiles are parabolic in shape with the same symmetry axis.

The heat of transport,  $Q^*$ , for carbon in vanadium as well as in V-Ti alloys is negative, i.e., carbon is transported toward the hotter regions of the specimen. The results of the thermotransport experiments for the entire series of alloys are given in Table 2, from which it is seen that  $Q^*$  for carbon changes from  $-42.27 \pm 0.5$  kJ/mol in vanadium to  $-13.97 \pm 1.50$  kJ/mol in the V-20.5 at.% Ti alloy, i.e., decreases in absolute magnitude with

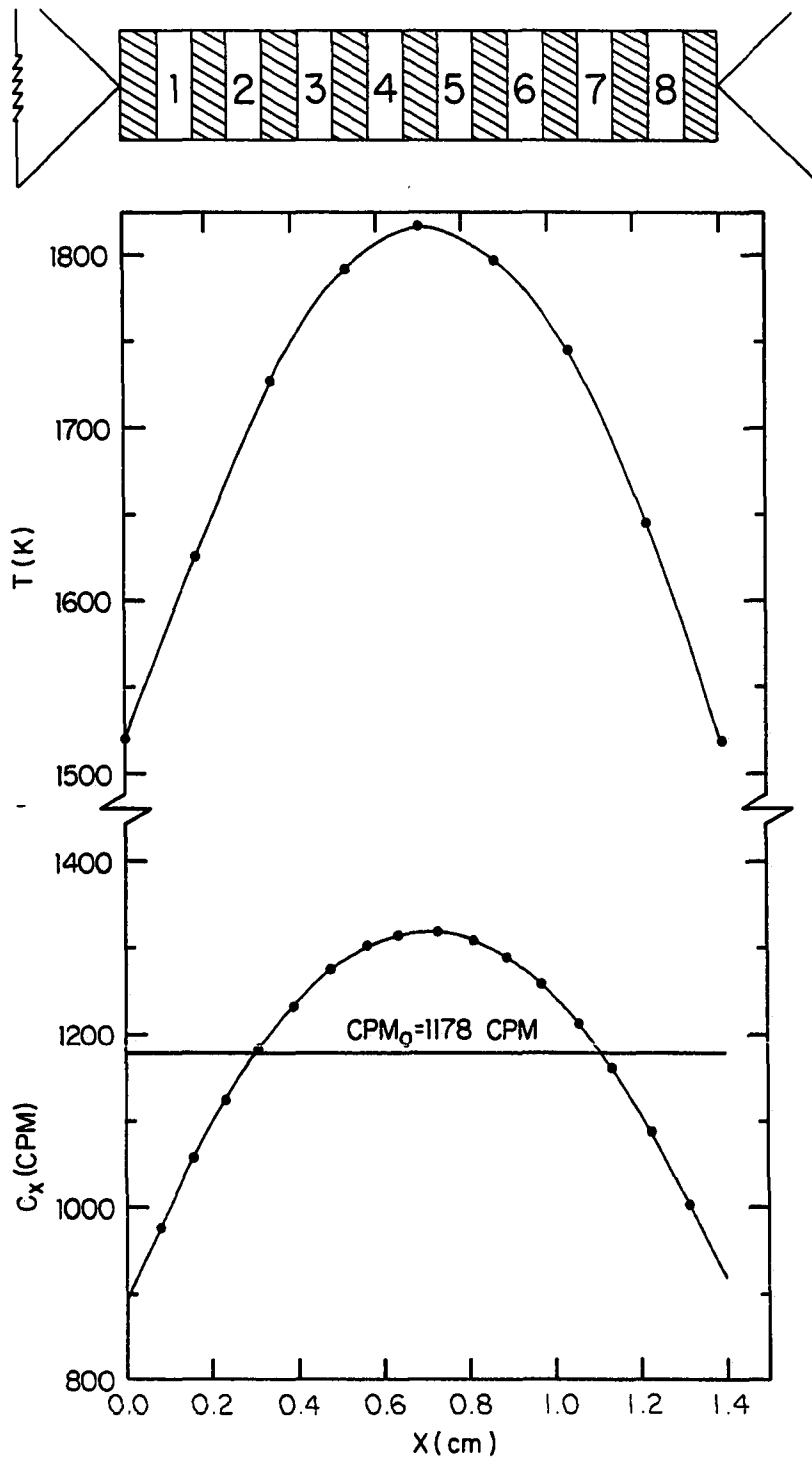


Figure 3. Temperature and concentration profiles, and segmented sketch of sample for V-1.1 at.% C thermotransport run

Table 2. Experimental conditions and results for thermotransport of carbon in vanadium and vanadium-titanium alloys

Titanium content (at.%)	Temperature range		Degree of steady state (%)	Material balance <sup>a</sup> (%)	Q* (kJ/mol)	Q* <sub>avg</sub> ± mean deviation (kJ/mol)
	Low (K)	High (K)				
0.0 <sup>b</sup>	~1220	~1273	--	--	--	-20.5 ± 4.2
0.0 <sup>c</sup>	~1030	~1243	--	--	--	-14.6
0.0 <sup>d</sup>	1433	1813	98.8	91	-42.40	-42.27 ± 0.50
0.0 <sup>d</sup>	1393	1844	99.1	93	-41.82	
0.0 <sup>e</sup>	1466	1854	99.8	93	-42.23	
0.0 <sup>e</sup>	1308	1652	99.1	92	-42.62	
1.1	1505	1851	99.0	94	-33.70	-34.70 ± 1.00
1.1	1545	1890	99.6	94	-35.69	
2.1	1518	1816	99.6	95	-27.62	-28.32 ± 0.70
2.1	1522	1843	99.5	90	-29.02	
5.3	1453	1891	99.4	96	-25.77	-25.34 ± 0.44
5.3	1541	1875	99.7	95	-24.90	
10.5	1674	1832	98.8	98	-15.98	-17.10 ± 1.12
10.5	1542	1881	99.4	96	-18.21	
20.5	1557	1834	99.4	96	-13.97	-13.97
100.0 <sup>b</sup>	--	--	--	--	--	-4.2 ± 4.2

<sup>a</sup>Obtained from a comparison of the area enclosed by concentration profile above initial counts per minute (CPM<sub>0</sub>) with that below it.

<sup>b</sup>Reference [36].

<sup>c</sup>Reference [37].

<sup>d</sup>Contains 0.038 at.% carbon.

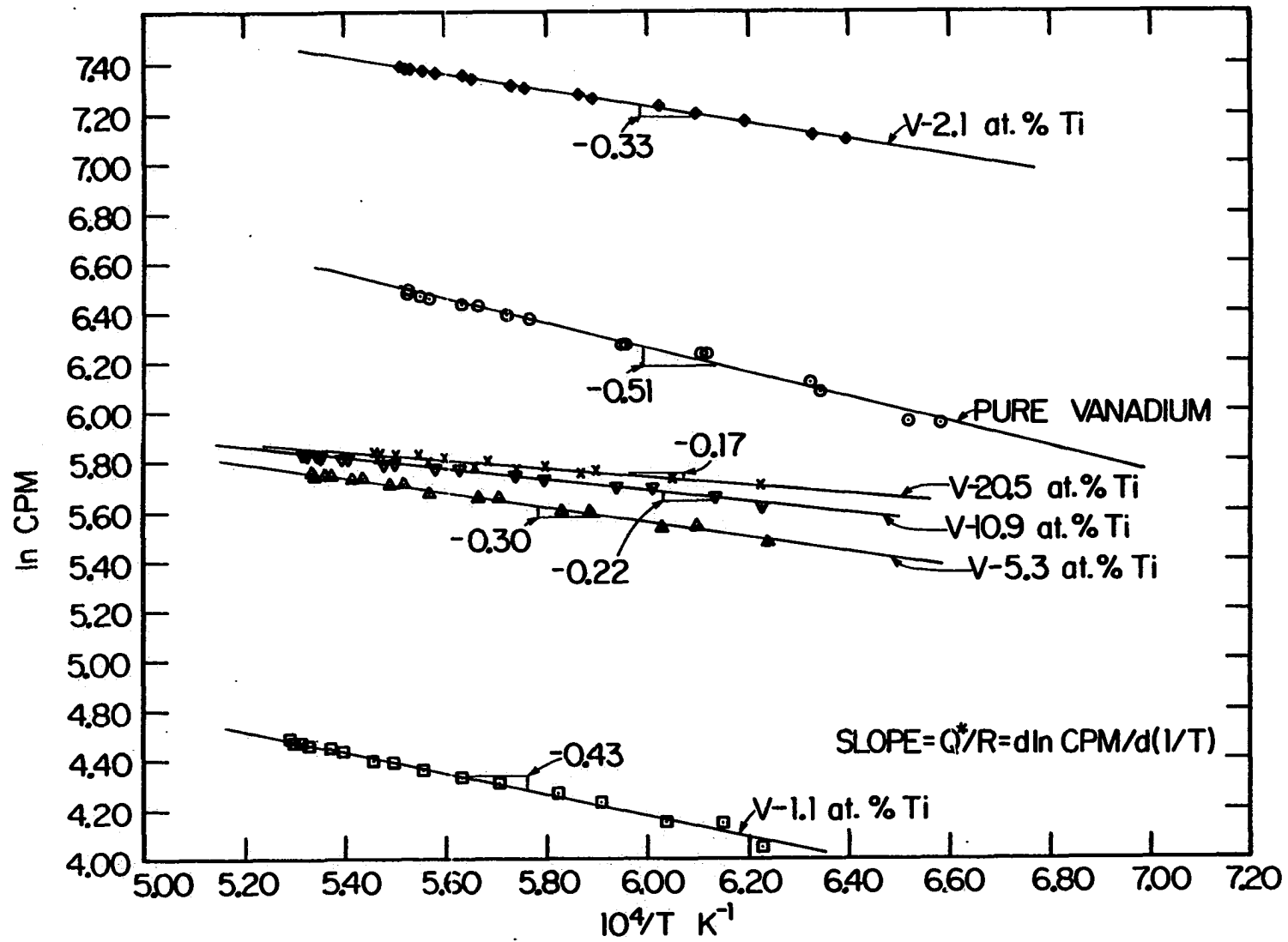
<sup>e</sup>Contains 0.457 at.% carbon.

increasing titanium content. This variation in  $Q^*$  can also be seen from the changes in the slopes of the plots of  $\ln CPM$  versus the reciprocal temperature for various V-Ti alloys in Figure 4.

### Diffusion

The concentration profile shown in Figure 5 and the plot of  $\text{erf}^{-1}[(C_x - C_M)/(C_2 - C_M)]$  versus the distance in Figure 6 for the V-20.5 at.% Ti alloy are typical of those obtained from all the diffusion experiments. The results obtained from the present study show that the activation energy for diffusion of carbon in vanadium increases from its reported value of 116.3 kJ/mol [7] to 188.5 kJ/mol with the addition of 20.5 at.% titanium. It must go through a maximum at this or a higher titanium concentration, since the literature value of the activation energy for diffusion of carbon in  $\beta$ -titanium [8] is 94.6 kJ/mol. This trend is apparent from a comparison of the slopes of the plots of  $\log D$  versus the reciprocal temperature for carbon diffusion in vanadium, V-10.5 at.% Ti and V-20.5 at.% Ti alloys, and  $\beta$ -titanium in Figure 7. There is also a marked effect of titanium additions on the pre-exponential factor,  $D_0$ , which increases from 0.0088 cm<sup>2</sup>/sec for carbon in pure vanadium [7] to 1.299 cm<sup>2</sup>/sec in V-20.5 at.% Ti. The reported value of  $D_0$  for carbon in  $\beta$ -titanium [8] is 0.006 cm<sup>2</sup>/sec. The above trends are also apparent from a summary of the diffusion results in Table 3, in which the thermotransport results are also included for ease in comparison.

Figure 4. Plots of  $\ln$  concentration (CPM) versus reciprocal temperature for thermotransport of carbon in vanadium and V-Ti alloys



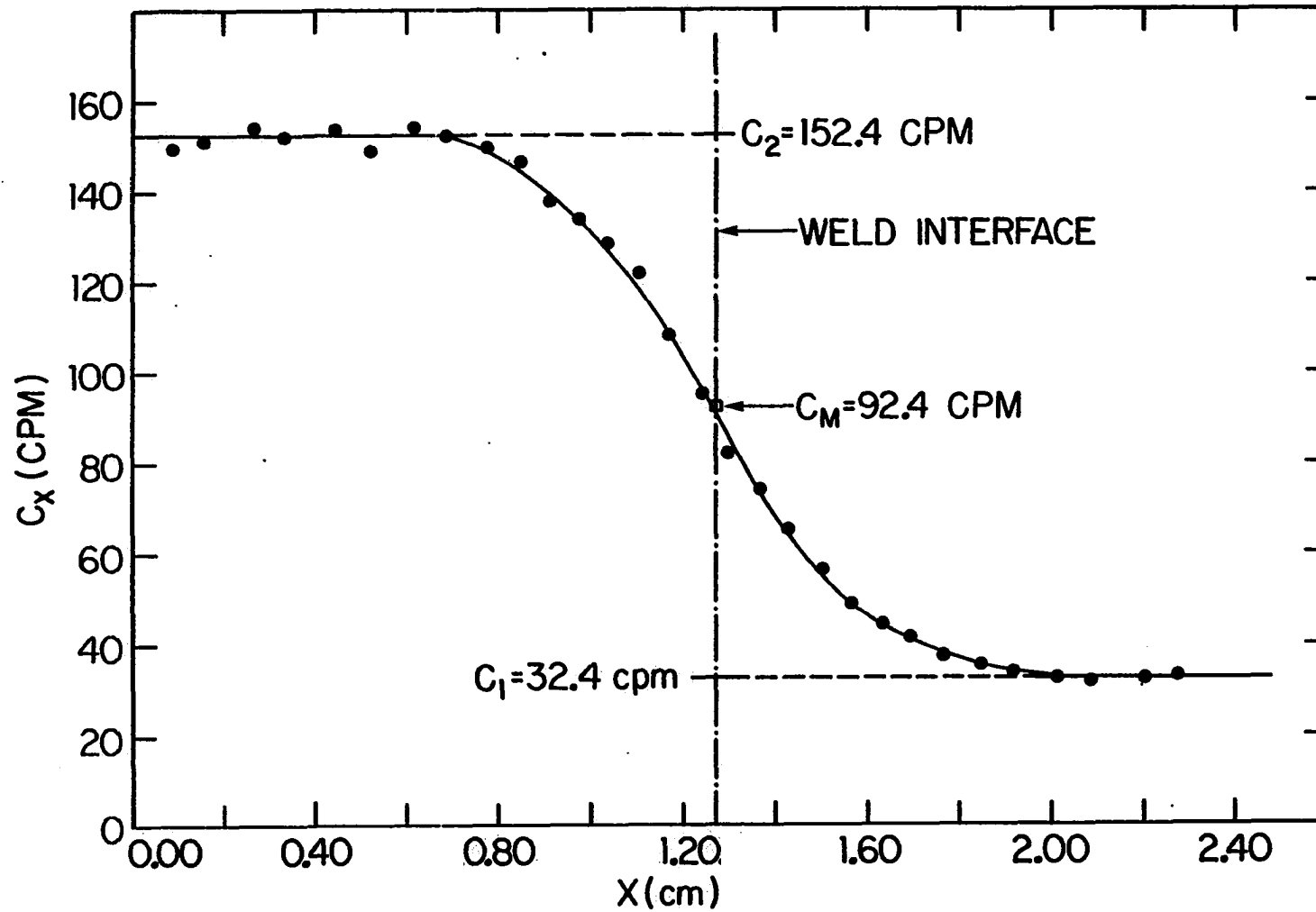


Figure 5. Concentration profile for diffusion of carbon in V-20.5 at.% Ti sample heated at 1423 K for 66 hours

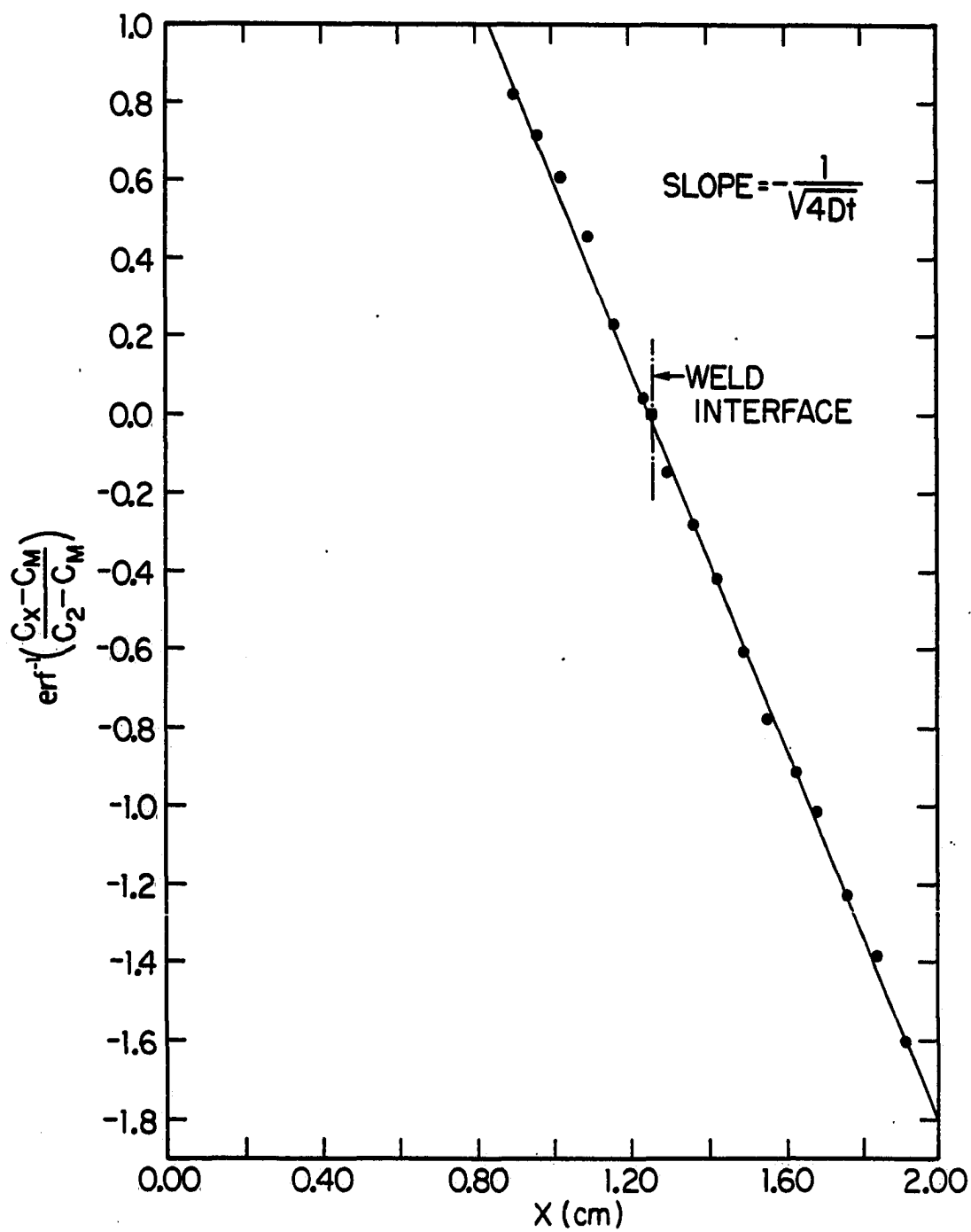


Figure 6. Plot of inverse error function versus distance for diffusion of carbon in V-20.5 at.% Ti sample heated at 1423 K for 66 hours

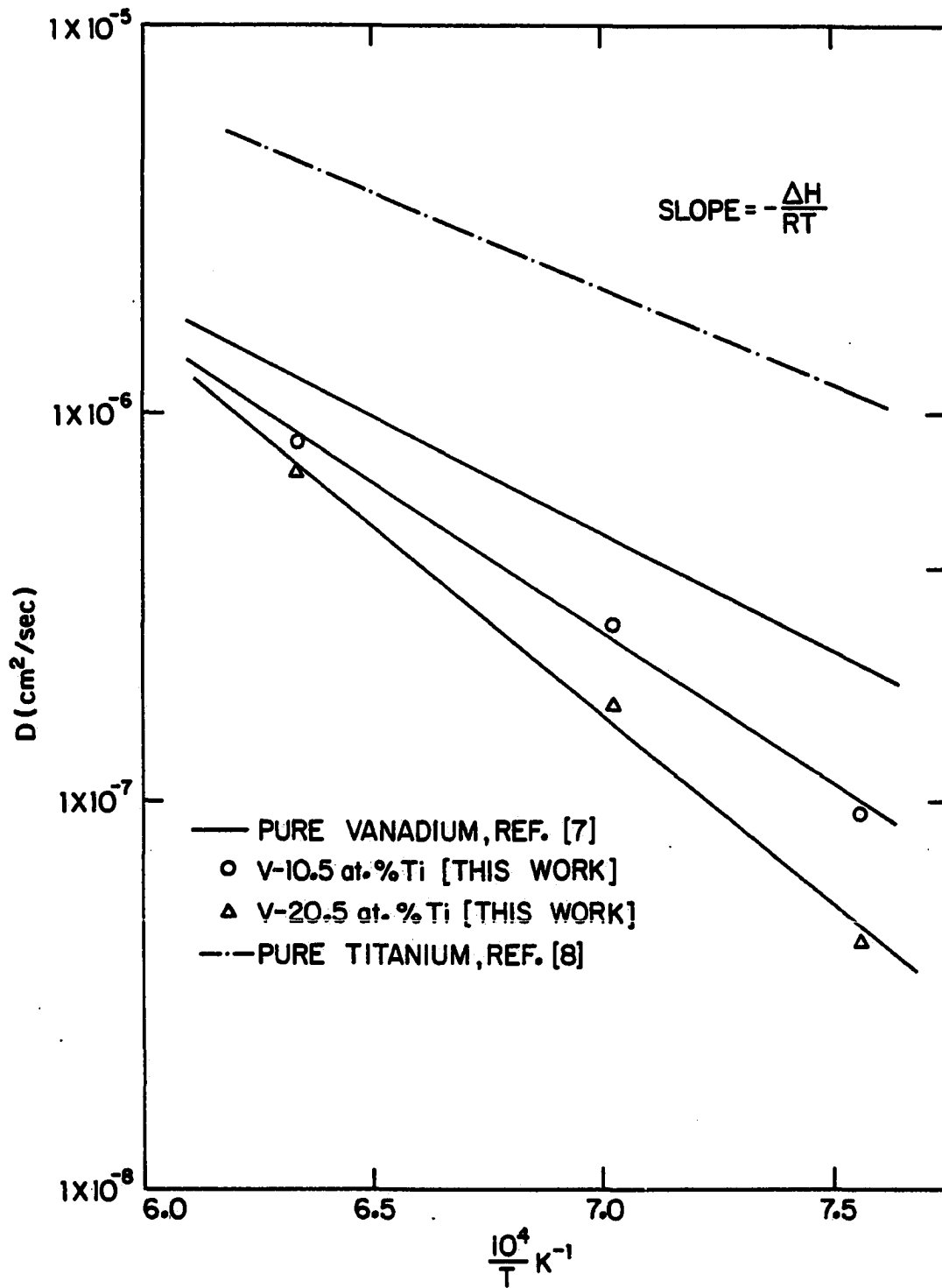


Figure 7. Arrhenius plots of diffusion coefficient versus reciprocal temperature for carbon in titanium, vanadium, and V-Ti alloys

Table 3. Heats of transport, activation energies and pre-exponential factors for diffusion of carbon in V-Ti alloys

Titanium content (at.%)	$Q^*$ (kJ/mol)	$\Delta H$ (kJ/mol)	$D_0$ ( $m^2/sec$ )	References	
				$Q^*$	$\Delta \bar{H}, D_0$
0.0	-42.27	116.29	$8.8 \times 10^{-7}$	This work	[7]
1.1	-34.70			This work	
2.1	-28.32			This work	
5.3	-25.34			This work	
10.5	-17.10	149.67	$8.1 \times 10^{-6}$	This work	This work
20.5	-13.97	188.49	$1.3 \times 10^{-4}$	This work	This work
100.0	- 4.20	94.56	$6.0 \times 10^{-7}$	[36]	[8]

## DISCUSSION OF RESULTS

The heat of transport for carbon in vanadium is negative, indicating that carbon is transported toward the hotter regions of a vanadium sample under a temperature gradient. However, the value of  $Q^*$  obtained in this investigation,  $-42.27$  kJ/mol, is considerably greater in magnitude than that reported by Shaw and Oates [36],  $-20.5$  kJ/mol, or Morozomi *et al.* [37],  $-14.6$  kJ/mol. The possibility that this discrepancy is attributable to a temperature dependence of  $Q^*$  was considered inasmuch as the two literature values were obtained from experiments performed in the temperature range of about 1023 to 1273 K, whereas the experiments in the present study were carried out at much higher temperatures. Such a temperature dependence of  $Q^*$  has been reported for oxygen in tantalum [38]. However, the values obtained for  $Q^*$  agreed to within  $\pm 1$  kJ/mol in the present study, even though the lower ends of the temperature ranges for different experiments varied from 1308 to 1466 K, and the higher ends from 1652 to 1854 K (Table 2). Furthermore, there was no indication of a deviation from linearity in the plots of  $\ln$  CPM versus the reciprocal temperature, although the high and low temperatures differed by as much as 450 degrees in a given experiment.

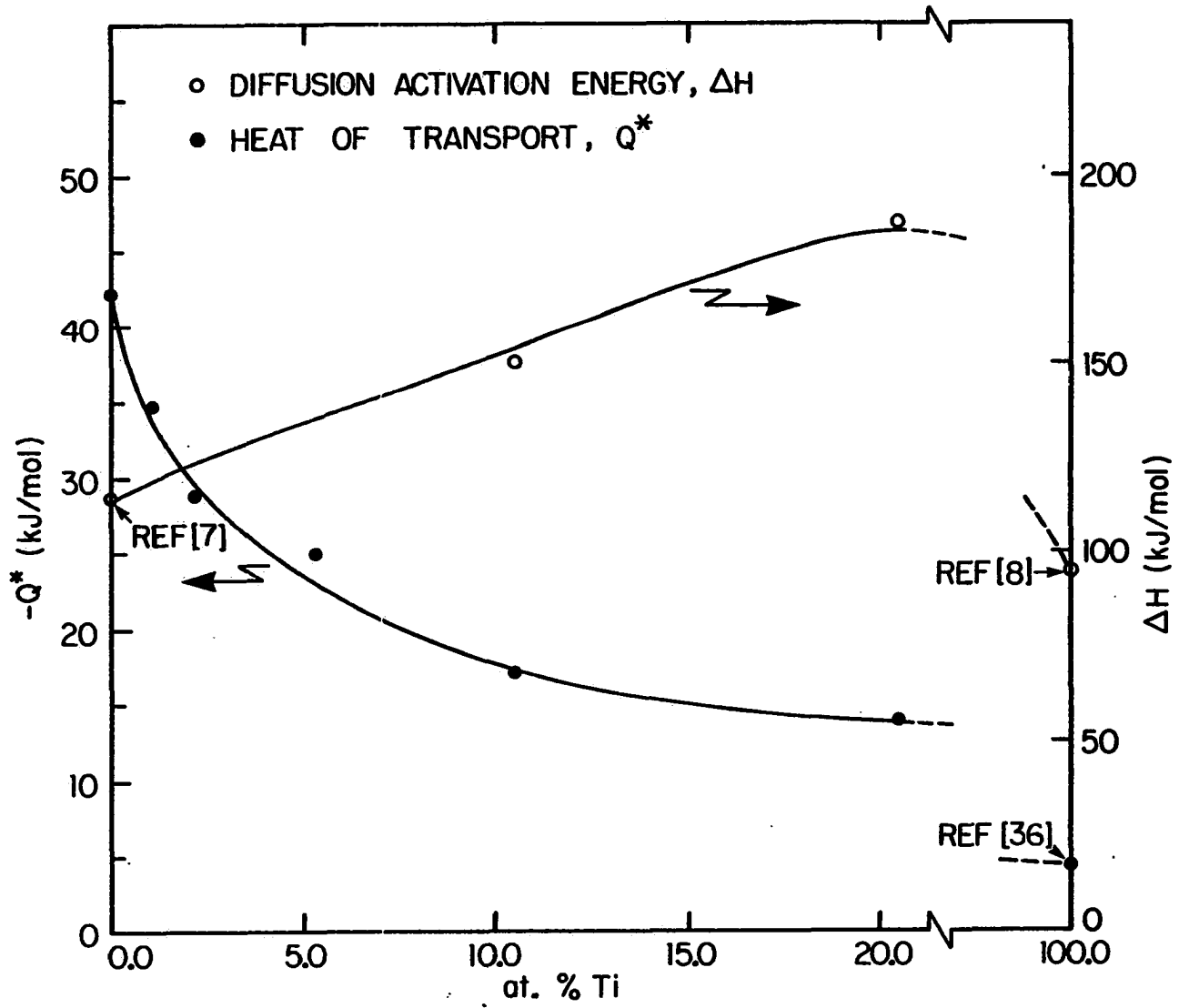
A concentration dependence of  $Q^*$ , which was reported to be the case for oxygen in tantalum [38], vanadium [39], and niobium [40], would be another possible explanation for this discrepancy. The carbon contents of the vanadium samples used in obtaining the literature

values, 0.024 [36] and 0.372 at.% [37], are comparable to those used in this investigation, namely, 0.037 and 0.457 at.%. However, as can be seen from Table 2, there is no measurable difference between the heats of transport obtained from these samples in this study.

The above discussion of experimental conditions and results indicates that the disagreement between the results obtained in this study and those of the previous investigators [36, 37] cannot be explained by either a temperature or concentration dependence of  $Q^*$  for carbon in vanadium. As was reported by the present authors [30] and mentioned earlier in this manuscript, in a system with a negative  $Q^*$ , one can obtain lower magnitudes, or even positive values for  $Q^*$ , erroneously depending on the severity of environmental effects. Therefore, this may be a likely explanation for the lower magnitude of the literature values. The results obtained in the present study were virtually free of any external effects and reproducible, and a material balance of 90% or better was obtained from each run (Table 2). No material balance was reported for the literature values.

The heat of transport for carbon in each of the V-Ti alloys is also negative, and its absolute magnitude decreases with increasing titanium content, as is seen from Table 3. It also shows that both the activation energy for diffusion,  $\Delta H$ , of carbon in vanadium and the pre-exponential factor,  $D_0$ , increase with increasing titanium content, at least to 20.5 at.% titanium. As can be seen from Figure 8, the decrease in the absolute magnitude of  $Q^*$  for carbon in vanadium with

**Figure 8. Variation of heat of transport, and activation energy for diffusion of carbon in vanadium with titanium concentration**



increasing titanium content up to 20.5 at.% titanium is monotonic, and would appear to approach the reported value in  $\beta$ -titanium. The activation energy for diffusion of carbon in vanadium, on the other hand, increases almost linearly from 116.3 kJ/mol [7] to 188.5 kJ/mol upon the addition of 20.5 at.% titanium, and must go through a maximum at some higher titanium concentration before decreasing to the literature value of 94.6 kJ/mol in  $\beta$ -titanium [8].

An examination of the driving forces discussed in an earlier section indicates that for the thermotransport of interstitial solutes in metals and alloys, the heat of transport can be expressed as

$$Q^* = Q_{in}^* + Q_{el}^* \quad (11)$$

At present, a separate determination of the contributions to  $Q^*$ , i.e.,  $Q_{in}^*$  and  $Q_{el}^*$ , is not possible from thermotransport experiments. However, their presence and significance can be deduced from a comparison of the effect of composition on  $Q^*$  with that on the characteristic parameters of other phenomena such as diffusion, thermoelectricity and electrotransport, of which the atomistic aspects are better developed. A comprehensive study concerning the effects of composition on all these phenomena in the same system has not been undertaken.

Peterson and Smith [9] studied the thermotransport of hydrogen and deuterium in V-Ti, V-Cr and V-Nb alloys. They reported  $Q^*$  to be

positive for hydrogen and deuterium in vanadium, and found it to increase in magnitude upon alloying with titanium, chromium, and niobium. They presented a model expressing  $Q^*$  as

$$Q^* = \Delta H + \delta \quad (12)$$

where  $\Delta H$  is the activation energy for diffusion, and  $\delta$  is a biasing term in the direction of a jump with respect to the temperature gradient. Their model is similar in form to Equation (11) with  $\Delta H$  representing the intrinsic contribution and  $\delta$  the others. In another study, Peterson and Herro [41] found that the activation energy for diffusion of hydrogen in vanadium increases monotonically with increasing titanium across the entire system, whereas  $Q^*$  for hydrogen in vanadium was reported [9] to increase with titanium content to a maximum at 20 at.% titanium. However, the magnitudes of changes in  $Q^*$  and  $\Delta H$  upon alloying were not equal, as is the case for carbon in V-Ti alloys in this study, indicating that the changes in  $\Delta H$  could not solely account for changes in  $Q^*$ .

In a system with a negative  $Q^*$ , there should be a driving force greater in magnitude than the intrinsic contribution,  $Q_{in}^*$ , but opposite in sign, since  $Q_{in}$  is always positive. This driving force should be the electronic contribution,  $Q_{el}^*$  in Equation (11). However, there is more evidence for the presence and significance of the electronic contribution than this simple deduction, as will be seen from the following discussions.

Kirchheim and Fromm [40], in an investigation concerning thermotransport of oxygen in tantalum and niobium, reported a negative  $Q^*$ , and found that it decreases in absolute magnitude with increasing oxygen content. They also found that the thermoelectric power,  $S$ , varies in a similar manner to  $Q^*$  with increasing oxygen concentration. Mathuni et al. [10], in their study of the effects of tungsten, rhenium and nitrogen additions on  $Q^*$  and  $S$  for oxygen in tantalum, reported that both parameters varied similarly upon alloying. They found a linear relationship between the heat of transport and thermoelectric power expressed as

$$Q^* = a + bS . \quad (13)$$

This is also similar in form to Equation (11). However, the changes in  $Q^*$  were not of the same magnitude as the corresponding changes in  $S$  upon alloying, indicating that changes in  $S$  alone cannot be responsible for changes in  $Q^*$ .

In an analysis of the driving forces in thermotransport, Huntington [16] calculated a large positive electronic contribution for the self-thermotransport in platinum. Similarly, Hehenkamp [1] calculated  $Q_{el}^*$  for both germanium in copper and tin in silver to be negative. He also reported that this contribution decreased in absolute magnitude monotonically with increased alloying. Furthermore, the empirical correlation between the sign of the characteristic parameter

of electrotransport,  $Z^*$ , and that of thermotransport,  $Q^*$ , [38] such that

$$\text{Sign } Q^* = - \text{Sign } Z^* \quad (14)$$

would seem to indicate that there are similarities in the driving forces of the electrotransport and thermotransport phenomena. Such a sign correlation has been confirmed experimentally in numerous interstitial-metal systems with very few exceptions [30, 36, 38].

The results and discussions presented above would indicate that both the intrinsic and electronic effects contribute to thermotransport. There is convincing evidence that the electronic contribution plays a significant role in determining the sign and magnitude of  $Q^*$ , as is evident from the sign correlation between  $Q^*$  and  $Z^*$ , and similarities in the effects of alloying on  $Q^*$  and  $S$ . There is experimental and theoretical evidence that the thermoelectric power,  $S$ , constitutes some portion of  $Q_{el}^*$ . Furthermore,  $Q_{el}^*$  must be the dominant contribution in thermotransport, especially when  $Q^*$  is negative. There is also experimental evidence indicating that the intrinsic contribution may be represented in part by activation energy for diffusion. However, as is seen from the above discussions, the changes in  $\Delta H$  or  $S$  alone cannot account for the changes in  $Q^*$ .

## CONCLUSIONS

From an examination of the results obtained in this investigation and the related studies, the following conclusions can be drawn.

1) The heats of transport for carbon in vanadium and V-Ti alloys are negative, indicating that carbon is transported toward the hotter regions.

2) The absolute magnitude of  $Q^*$  for carbon in vanadium decreases with increasing titanium additions.

3) The activation energy for diffusion of carbon in vanadium increases almost linearly with increasing titanium content up to 20.5 at.% titanium, and must go through a maximum at this or a higher titanium concentration.

4) Although there is evidence that  $\Delta H$  and  $S$  constitute, in part, the intrinsic and electronic contributions, respectively, changes in either parameter alone cannot account for changes in  $Q^*$  upon alloying additions.

5) A comprehensive study concerning the effects of composition on  $Q^*$ ,  $S$ ,  $\Delta H$  and  $Z^*$  in a single system is needed to better evaluate the existing models, and understand the atomistic aspects of the thermotransport phenomenon.

## REFERENCES CITED

1. T. Hehenkamp, in Electro- and Thermo-transport in Metals and Alloys, edited by R. E. Hummel and H. B. Huntington (AIME, Inc., New York, 1977), p. 68.
2. W. Rostoker, A. S. Yamamoto and R. E. Riley, Trans. ASM 48, 560 (1956).
3. B. R. Bajala and R. S. Van Thyne, J. Less-Common Metals 3, 489 (1961).
4. R. C. Hought and S. M. Grimes, in Neutron Data of Structural Materials for Fast Reactors, edited by K. H. Böckhoff (Pergamon Press, New York, 1979), p. 312.
5. A. Smith, R. McKnight and D. Smith, in Neutron Data of Structural Materials for Fast Reactors, edited by K. H. Böckhoff (Pergamon Press, New York, 1979), p. 374.
6. J. L. Murray, Bulletin of Alloy Phase Diagrams 2, No. 1, 48 (1981).
7. F. A. Schmidt and J. C. Warner, J. Less-Common Metals 26, 325 (1972).
8. O. N. Carlson, F. A. Schmidt and R. R. Lichtenberg, Metall. Trans. A 6A, 725 (1975).
9. D. T. Peterson and M. F. Smith, Metall. Trans. A 13A, 821 (1982).
10. J. Mathuni, R. Kirchheim and E. Fromm, Acta Metall. 27, 1665 (1979).
11. H. Wever, Z. Metallkd. 74, 1 (1983).
12. R. E. Howard and J. R. Manning, J. Chem. Phys. 36, No. 4, 910 (1962).
13. V. B. Fiks, Sov. Phys.-Solid State 5, No. 12, 2549 (1964).
14. A. R. Allnatt and A. V. Chadwick, Chem. Rev. 67, 681 (1967).
15. M. Gerl, J. Phys. Chem. Solids 27, 725 (1967).
16. H. B. Huntington, J. Phys. Chem. Solids 29, 1641 (1968).
17. E. Fromm and W. Lohnert, Z. Metallkd. 62, 463 (1971).
18. H. B. Huntington, in Diffusion (ASM, Metals Park, Ohio, 1973), p. 155.

19. R. S. Sorbello, in Electro- and Thermo-transport in Metals and Alloys, edited by R. E. Hummel and H. B. Huntington (AIME, Inc., New York, 1977), p. 2.
20. J. Mathuni, R. Kirchheim and E. Fromm, *Scr. Metall.* 13, 631 (1979).
21. W. Jones, *J. Phys. F: Met. Phys.* 12, 87 (1982).
22. R. Kikuchi, T. Ishikawa and H. Sato, *Physica* 123A, 227 (1984).
23. G. B. Kale, S. K. Khera and G. P. Tiwari, *Trans. Indian Inst. Met.* 34, No. 3, 239 (1981).
24. S. R. DeGroot, *Thermodynamics of Irreversible Processes* (Interscience, New York, 1952).
25. I. Prigogine, Introduction to Thermodynamics of Irreversible Processes, 2nd Edition (Interscience, New York, 1961).
26. G. Grube and A. Jedele, *Z. Electrochem.* 38, 799 (1932).
27. J. D. Verhoeven, Fundamentals of Physical Metallurgy (John Wiley and Sons, Inc., New York, 1975), p. 142.
28. P. G. Shewmon, Diffusion in Solids (McGraw-Hill, New York, 1963), p. 14.
29. D. T. Peterson, R. G. Clark and W. A. Stensland, *J. Less-Common Metals* 30, 169 (1973).
30. O. N. Carlson, F. A. Schmidt and M. Uz, *J. Less-Common Metals* 79, 97 (1981).
31. Selected Values of the Thermodynamic Properties of the Elements, prepared by P. D. Desai, D. T. Hawkins, M. Gleiser, K. K. Kelley and D. D. Wagman (ASM, Metals Park, Ohio, 1973), pp. 519, 545.
32. O. Yoshinari, T. Kemro, K. Syma and M. Koiwa, *J. Less-Common Metals* 81, 239 (1981).
33. J. C. Warner, Databook JCW-1, Department of Materials Science and Engineering, Iowa State University, and Ames Laboratory, Ames, Iowa (unpublished data, 1964), p. 10.
34. A. Ghaneya and O. N. Carlson, Department of Materials Science and Engineering, Iowa State University, and Ames Laboratory, Ames, Iowa (unpublished data, 1983).

35. M. Uz and O. N. Carlson, Department of Materials Science and Engineering, Iowa State University, and Ames Laboratory, Ames, Iowa (Section II in this thesis).
36. J. G. Shaw and W. A. Oates, Metall. Trans. 2, 2127 (1971).
37. S. Morozumi, S. Goto and T. Yoshida, Scr. Metall. 10, 537 (1976).
38. R. Kirchheim and E. Fromm, High Temperatures - High Pressures 6, 329 (1974).
39. J. Mathuni, O. N. Carlson, E. Fromm and R. Kirchheim, Metall. Trans. A 7A, 977 (1976).
40. R. Kirchheim and E. Fromm, Acta Metall. 22, 1543 (1974).
41. D. T. Peterson and H. M. Herro, Department of Materials Science and Engineering, Iowa State University, and Ames Laboratory, Ames, Iowa, Private Communication, 1983.

**SECTION II. THERMOTRANSPORT OF CARBON IN TWO-PHASE  
VANADIUM-CARBON AND NIOBIUM-CARBON ALLOYS**

## INTRODUCTION

The mass transport phenomenon that occurs in a solid solution system due to an applied temperature gradient, resulting in the redistribution of mobile components, is known as thermotransport. It is also referred to as thermal migration, or sometimes as thermal diffusion. It usually causes a concentration gradient with respect to one or more of the components to develop, which may alter the physical and mechanical properties of the material rather significantly [1]. Since many metals and alloys used at elevated temperatures are being subjected to progressively higher temperatures, hence greater temperature gradients, thermotransport is of increasing technological interest.

Many engineering materials are multicomponent alloys that have a high affinity for interstitial impurities such as carbon, oxygen, hydrogen and nitrogen. Thus, in a contaminative environment at high temperatures, a material can pick up and become saturated with a particular impurity. The presence of a temperature gradient would then result in a nonuniform distribution of the impurity, leading to a gradation of properties in the material. Furthermore, the presence of second phase particles gives rise to considerable changes in the thermotransport behavior of an interstitial solute in the metal or alloy, as has been reported for carbon in  $\alpha$ -iron [2] and Fe-Ni alloys [3], and hydrogen in zircaloy [4]. Therefore, studies concerning the effects of second phase particles on the thermotransport of a solute in metals and alloys should also be of technological interest.

Various vanadium- and niobium-base alloys are candidates for some high temperature applications, and are considered as alternate structural materials for fast breeder nuclear and fusion reactors [5-7], where large temperature gradients exist. Furthermore, the niobium-base alloys are candidates for space nuclear power applications as structural and fuel cladding materials [8].

Almost all of the previous thermotransport studies have been made on dilute binary alloys [9]. The number of investigations involving ternary systems [10-12] is quite limited, as is the case for studies of the effects of second phase particles on the transport phenomenon [2-4, 13, 14]. This study consists of a systematic investigation of the effects of divanadium and diniobium carbide ( $V_2C$  and  $Nb_2C$ ) particles on the mass transport of carbon in vanadium and niobium under a temperature gradient. Thermotransport of carbon in vanadium [12] and niobium [15] has been made under one-phase conditions, also.

## THEORETICAL

The theory of, and the driving forces in thermotransport have been analyzed in some detail, and the relevant references are given in another publication by the authors [12]. In the present manuscript, the equation for thermotransport in a homogeneous binary alloy is modified to describe the mass transport under a temperature gradient in the presence of second phase particles.

The phenomenological equations for thermotransport have been derived using the principles of irreversible thermodynamics [16-18]. Thermotransport experiments are often carried out under a one-dimensional temperature gradient in the absence of any external fields, such as an applied electric field. Thus, the governing equation for thermotransport in a binary solid solution containing only one mobile specie,  $i$ , whose activity coefficient is independent of concentration, can be expressed as

$$J_i = - \frac{C_i D_i}{RT} \left[ \frac{RT}{C_i} \frac{dC_i}{dX} + \frac{Q^*}{T} \frac{dT}{dX} \right], \quad (1)$$

where  $D_i$  and  $C_i$  are the diffusion coefficient and concentration of  $i$ , respectively,  $R$  is the gas constant,  $T$  is the absolute temperature, and  $Q^*$  is the heat of transport. In Equation (1), the first and second terms within the brackets represent the forces due to the concentration and temperature gradients, respectively.

The heat of transport is usually determined from one-phase thermotransport experiments at or near steady state; hence, with the

use of the identities  $(1/C_i)(dC_i/dX) \equiv (d \ln C_i/dX)$  and  $(1/T^2)(dT/dX) \equiv -d(1/T)/dX$ , and setting  $J_i = 0$  in Equation (1), one obtains

$$Q^* = R \frac{d \ln C_i}{d\left(\frac{1}{T}\right)} . \quad (2)$$

As can be seen from Equation (2),  $Q^*$  can be obtained from a plot of  $\ln C_i$  versus the reciprocal temperature. Its sign and magnitude represent the direction and magnitude of solute transport, with a positive sign indicating migration toward the colder regions of the specimen.

Although Equation (1) was originally derived for one-phase thermotransport, it can be modified to describe the mass transport in a two-phase sample under a temperature gradient. In doing so, one assumes that (i) the only mobile specie is the interstitial solute atom, of which the amount in solid solution is fixed by its solubility limit in the matrix, (ii) there is local equilibrium between the interstitial atoms in solid solution and those in the second phase particles, and (iii) the difference between the molar volumes of the two phases is negligible. Furthermore, one should take into account cross-sectional area effect discussed by Okafor et al. [3], which follows from the assumption (i) above. In other words, the diffusivity of the interstitial in the second phase is negligible relative to that in the matrix, which should be valid in the present study. At 1500 K for example, the diffusion coefficient for carbon is  $1.2 \times 10^{-7} \text{ cm}^2/\text{sec}$  [19]

in niobium, whereas it is of the order of  $10^{-13}$  cm<sup>2</sup>/sec in Nb<sub>2</sub>C [20]. Also, at the same temperature, the diffusion coefficient of carbon in vanadium is  $7.8 \times 10^{-7}$  cm<sup>2</sup>/sec [21], and although no data are available, it should be of similar order in V<sub>2</sub>C as in Nb<sub>2</sub>C. As a consequence of the above conditions, an increase in the fraction of the cross-sectional area occupied by the second phase particles is accompanied by a decrease in the net total flux of the solute in a region. Hence, a factor  $a_i$ , defined as that fraction of the cross-sectional area of the specimen represented by the solid solution phase, must be introduced into Equation (1) to give a better representation of the mass transport phenomenon under a temperature gradient. Thus, Equation (1) can be rewritten as

$$J_i = - \frac{D_i C_i a_i}{R} \left[ \frac{R}{C_i} \frac{dC_i}{dX} + \frac{Q^*}{T^2} \frac{dT}{dX} \right] \quad (3)$$

The assumption that the solute transport takes place only through the matrix phase was also made by the aforementioned authors in their studies; however, unlike Okafor et al. [3], the others [2, 4, 13, 14] have not taken the  $a_i$  factor into account.

In Equation (3),  $a_i$ , of course, is unity for the case of one-phase thermotransport; however, for the two-phase case, it is defined by the lever rule at a given concentration and temperature. The solid solubility limit for a solute in a binary system can be described by an Arrhenius-type equation,  $C_i = C_o \exp(-\Delta\bar{H}/RT)$ , where  $\Delta\bar{H}$  is the partial

molar enthalpy of solution for the solute. Hence, replacing  $(1/C_1)(dC_1/dX)$  by  $(\Delta\bar{H}/RT^2)(dT/dX)$  in Equation (1), one obtains

$$J_i = - \frac{D_i C_i a_i}{RT^2} (\Delta\bar{H} + Q^*) \frac{dT}{dX} , \quad (4)$$

which is the governing equation for mass transport in a two-phase sample under a temperature gradient. As is seen from the equation, the direction and magnitude of the net mass transport are then represented by the sign and magnitude of the quantity  $(\Delta\bar{H} + Q^*)$ .

## EXPERIMENTAL

## Materials and Apparatus

Vanadium metal was obtained from the Materials Preparation Center of the Ames Laboratory, and niobium metal from Kawecki-Berylco Industries, Inc. The total amount of metallic impurities in the vanadium, as well as in the niobium, was less than 0.05 at.%. Each metal was electron-beam melted under a pressure of about  $10^{-6}$  Torr to remove volatile impurities, and then doped with  $^{14}\text{C}$  by arc melting in a purified argon atmosphere. Spectroscopic grade graphite was added to each of the doped metals in a separate arc melting step to obtain the samples of higher carbon content. The samples were subsequently swaged into rods of about 0.25 cm in diameter, followed by deoxidation with calcium, as described by Peterson *et al.* [22]. The carbon, oxygen and nitrogen contents of the alloys used in this study are given in Table 1. The lengths of the samples varied from 1.5 to 1.9 cm. Each was surface cleaned by electropolishing in a methanol-sulfuric acid solution before being heated.

The apparatus used in this investigation has been described in detail in another paper by the authors [12], so will only be described briefly here. It consisted of an ultrahigh vacuum chamber, and a gettering chamber attached to it. The latter was a stainless steel tube filled with molecular sieve material capable of adsorbing hydrogen-, carbon-, nitrogen- and oxygen-bearing gases at liquid nitrogen temperature. This was used to further purify the laboratory-grade

Table 1. Carbon, oxygen and nitrogen concentrations of niobium and vanadium

Matrix metal	Impurity concentration (at.%)		
	Carbon <sup>a</sup>	Oxygen <sup>b</sup>	Nitrogen <sup>b</sup>
Niobium	0.347	0.010	0.006
Niobium	1.936	0.020	0.047
Vanadium	0.457	0.007	0.054
Vanadium	2.388	0.012	0.062

<sup>a</sup>Combustion chromatographic analysis.

<sup>b</sup>Vacuum fusion analysis.

helium gas prior to admission to the sample chamber. The sample was supported between two tapered tungsten adapters attached to water-cooled copper electrodes, and was heated by internal resistance using an a.c. power source. The temperature of the specimen was measured through a viewing port by an optical pyrometer that could be rotated on a base equipped with a vernier scale.

### Procedure

#### Data acquisition

All of the transport runs on V-C alloys, and one high-temperature run on a Nb-C alloy were carried out under a partial pressure of purified helium due to relatively high vapor pressures of the metals. The other Nb-C samples were heated under a pressure of the order of  $10^{-9}$  Torr. The

temperature measurements were made on the sample surface at equidistant points along its length. Each reading was corrected for the emissivity, which has been reported to be  $T_t = 1.083 T_s - 27.5$  for the V-C alloys [23], and determined in this investigation to be  $T_t = 1.136 T_s - 73$  for the Nb-C alloys, where  $T_t$  is the true temperature in  $^{\circ}\text{C}$ , and  $T_s$  is the surface temperature corrected for sight-glass absorption ( $\sim 16^{\circ}\text{C}$ ).

Following each run, the sample was ground along its entire length to obtain a flat surface. This surface was then mechanically polished, and/or etched, for metallographic examination of the sample. From such studies, it was possible to determine quite precisely the location of the boundary between the one- and two-phase regions of a partially two-phase sample. A diamond saw was used to cut each sample into 8-12 segments, which were subsequently ground through 600 grit to a nearly uniform thickness. A metallographic examination of the segments was also made for various V-C and Nb-C samples.

The concentration profile for each sample was determined from the  $\beta$ -activity of a uniform area of the ends of the segments. The  $\beta$ -activity, i.e. counts per minute (CPM), was then converted to atom percent by use of the relationship

$$\frac{C_x}{C_o} = \frac{\text{CPM}_x}{\text{CPM}_o} \quad (5)$$

In this equation,  $\text{CPM}_x$  is the  $\beta$ -activity of a cross-sectional area at a distance  $X$  along the sample,  $C_x$  is the corresponding carbon

concentration in atom percent,  $CPM_0$  is the initial  $\beta$ -activity of a given alloy, and  $C_0$  is its initial concentration as determined from combustion chromatographic analysis. As can be seen from Table 2, the concentration of each segment of one-half of a Nb-1.936 at.% C sample (Expt. 14) determined from its  $\beta$ -activity using Equation (5) is in good agreement with the analytically obtained concentration of the segment.

#### Calculation of concentration profiles

The concentration profiles for the mass transport of carbon in vanadium and niobium under a temperature gradient were calculated employing an explicit, single-step finite difference method. A similar method was used by Marino [14] and Okafor *et al.* [3] for different systems. Here, a model based on Equation (3), together with the assumptions made for its application to the two-phase mass transport, that led to Equation (4), was used as described below.

- a) For the one-phase case,  $a_1 = 1$ . For the two-phase case, however, it is less than unity.
- b) It is assumed that the transport of carbon takes place only in the matrix phase.
- c) The second phase particles (carbides) act as sources and sinks for carbon in solid solution.
- d) For carbon,  $D = 0.01 \exp(-141.9 \text{ kJ}\cdot\text{mol}^{-1}/RT)$  [19] and  $Q^* = -54.8 \text{ kJ/mol}$  [14] in niobium, and  $D = 0.008 \exp(-116.3 \text{ kJ}\cdot\text{mol}^{-1}/RT)$  [21] and  $Q^* = -42.3 \text{ kJ/mol}$  [12] in vanadium (Table 3).

Table 2. Comparison of analyzed carbon concentrations to those calculated from  $\beta$ -activity of segments from a Nb-1.936 at.% C sample (Expt. 14)

Segment no.	$\beta$ -activity (CPM)			Concentration (at.%)	
	Left side	Right side	Average	Calculated <sup>a</sup>	Analyzed <sup>b</sup>
7	296	318	307	1.10	1.06 $\pm$ 0.03
8	348	444	396	1.42	1.50 $\pm$ 0.03
9	532	592	562	2.01	1.99 $\pm$ 0.03
10	625	666	646	2.32	2.34 $\pm$ 0.03
11	648	639	644	2.31	2.31 $\pm$ 0.03
12	624	596	610	2.19	2.19 $\pm$ 0.03

<sup>a</sup>Calculated from average  $\beta$ -activity of a segment using Equation (5),  $CPM_0 = 540$ .

<sup>b</sup>Combustion chromatographic analysis.

Table 3. Diffusion and thermotransport data for carbon in vanadium and niobium

Metal	$D_o$ (m <sup>2</sup> /sec)	$\Delta H$ (kJ/mol)	$Q^*$ (kJ/mol)	References	
				H, $D_o$	$Q^*$
Niobium	$1.0 \times 10^{-6}$	141.9	-54.8	[19]	[15]
Vanadium	$8.8 \times 10^{-7}$	116.3	-42.3	[21]	[12]

d) When the carbon concentration exceeds the solid solubility limit,

1) its concentration in the matrix is fixed by

$$C_i = 4467 \exp(-145.5 \text{ kJ}\cdot\text{mol}^{-1}/RT) \text{ at.}\% \text{ in niobium [24],}$$

$$\text{and } C_i = 827 \exp(-86.8 \text{ kJ}\cdot\text{mol}^{-1}/RT) \text{ at.}\% \text{ in}$$

vanadium, as determined in this study by a method

that will be discussed in a later section; and

2) the area fraction of the matrix phase,  $a_i$ , is defined

$$\text{by the lever rule as } a_i = [C(\text{carb.}) - \bar{C}_i] / [C(\text{carb.}) - C_i],$$

where  $C(\text{carb.}) \approx 31.0 \text{ at.}\%$  for carbon in niobium [25],

$$\text{and } C(\text{carb.}) \approx 22 \exp(3.6 \text{ kJ}\cdot\text{mol}^{-1}/RT) \text{ at.}\% \text{ in}$$

vanadium [26], where  $\bar{C}_i$  is the overall carbon

concentration at a location along the sample, and  $C_i$

is the solubility limit determined from equations in

item 1 above at the corresponding temperature (Table 4).

A detailed analysis of the calculation of profiles resulting from the one- and two-phase thermotransport of interstitial solutes is given in the Appendix.

Table 4. Solvus data for M/M<sub>2</sub>C and M<sub>2</sub>C/M phase boundaries for V-C and Nb-C systems

Metal (M)	M/M <sub>2</sub> C		M <sub>2</sub> C/M		References	
	C <sub>o</sub> (at.%)	ΔH̄ (kJ/mol)	C <sub>o</sub> (at.%)	ΔH̄ (kJ/mol)	M/M <sub>2</sub> C	M <sub>2</sub> C/M
Niobium	4467	145.5	31.0	0	[24]	[25]
Vanadium	827	86.8	22.0	-3.6	[This work]	[26]

#### The role of second phase particles

A series of experiments was carried out to determine the behavior of the second phase particles in two-phase mass transport under a temperature gradient. For this purpose, several microhardness indentations were made on the mechanically polished surface along the length of a V-2.388 at.% C specimen heated under a temperature gradient for 26 hours. Consequently, the sample was electropolished in a sulfuric acid-methanol solution, and a micrograph of the area surrounding each indentation was taken at 400X. The specimen was then heated under the same temperature gradient for an additional 5 hours, and the area surrounding each indentation was rephotographed at the same magnification. In this way, a particle in a given location could be identified, and any change in its shape, size and/or location with respect to each indentation could be followed.

## RESULTS

## Temperature Profiles

In each experiment, the temperature profile was parabolic in shape with the highest temperature, or the symmetry axis at the midpoint of the specimen. It was fitted to a cubic equation of the form

$$T = T_0 + aX + bX^2 + cX^3 \quad (6)$$

where  $T$  is the true, or corrected temperature at any distance  $X$  along the sample in the direction of the temperature gradient, and  $T_0$ ,  $a$ ,  $b$  and  $c$  are constants. The temperature profile (both calculated and experimental) shown in Figure 1 is representative of those employed in this investigation.

## Carbon Mass Transport in Vanadium

The results of the studies of the mass transport of carbon in vanadium under a temperature gradient are summarized in Table 5. As can be seen from a comparison of the 7th and 8th columns of the table, the fraction of the sample in the two-phase condition was always less at the end of a run than that at the start.

The temperature range with respect to the solvus line, and the corresponding concentration profiles (calculated and experimentally determined) are shown in Figure 2(a) and 2(b), respectively, for each of the experiments on the V-0.457 at.% C alloy (Expts. 1-4). The

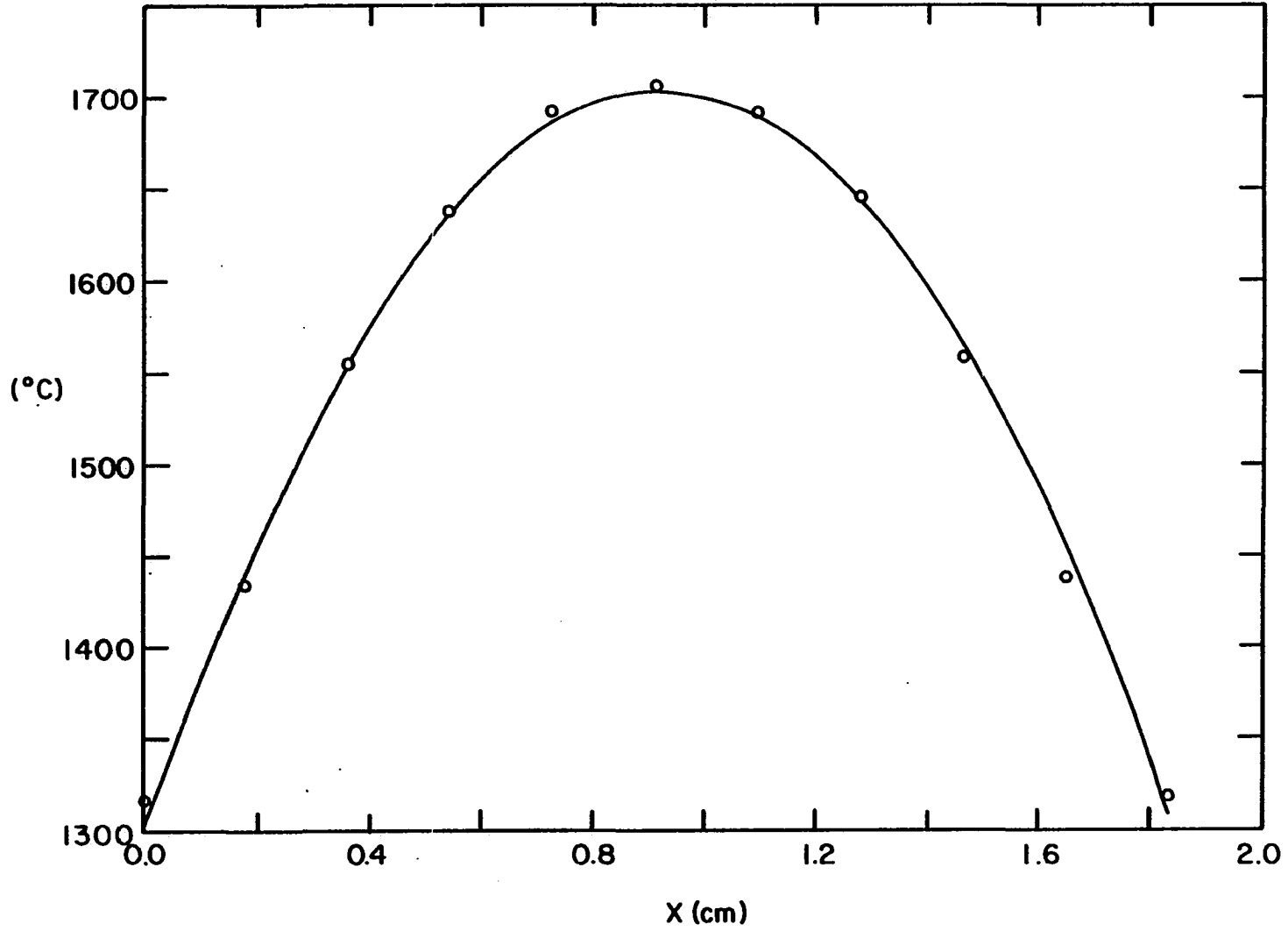


Figure 1. Temperature profile for Nb-1.936 at.% C sample (Expt. 14). (o = experimental; — = calculated)

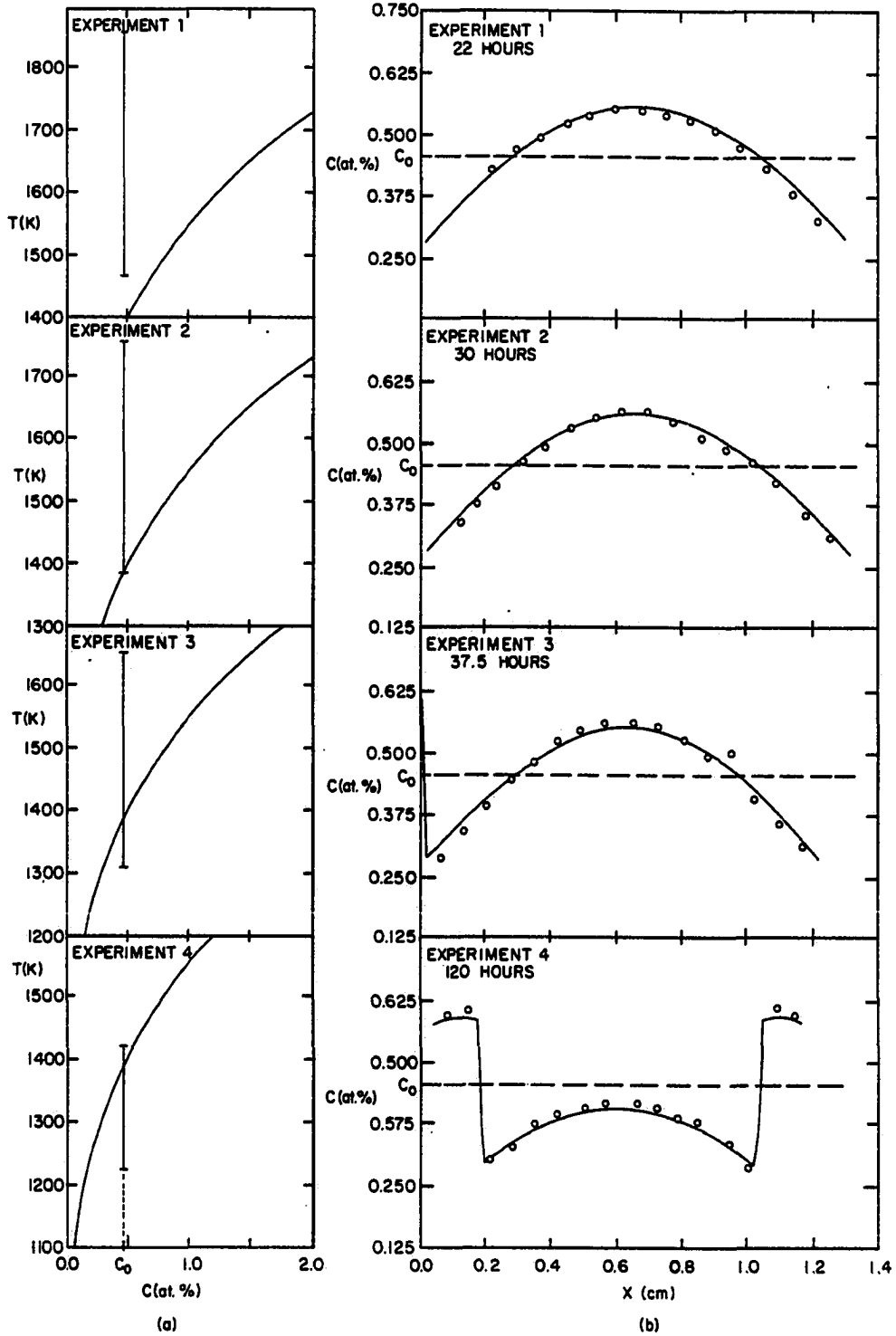
Table 5. Summary of experimental results for mass transport of carbon in vanadium under a temperature gradient

Experiment number	Carbon concentration (at.%)	Temperature range (K)			Temperature at solubility limit (K)	Heating period (hours)	% of sample in two-phase condition <sup>a</sup>		Q <sub>app</sub> <sup>* b</sup> (kJ/mol)
		High	Low				Initial	Final	
			Left	Right					
1	0.457	1854	1466	1479	1391	22.0	--	--	-42.2
2	0.457	1755	1400	1389	1391	30.0	<1	--	-43.1
3	0.457	1652	1308	1338	1391	37.5	13	<1	-42.3
4	0.457	1421	1222	1223	1391	120.0	67	30	-50.2
5	2.388	1748	1318	1318	1878	31.0	100	46	-58.6
6	2.388	1692	1334	1315	1878	42.5	100	56	-64.8
7	2.388	1630	1291	1280	1878	80.0	100	53	-52.3
8	2.388	1584	1256	1262	1878	78.0	100	100	--
9	2.388	1558	1242	1274	1878	144.0	100	75	--

<sup>a</sup>Determined from ratio of sample length below temperature of solubility limit for a given carbon concentration to its total length.

<sup>b</sup>Obtained from slope of a plot of  $\ln C$  versus reciprocal temperature as determined by least squares analysis of data from one-phase regions of partially two-phase samples.

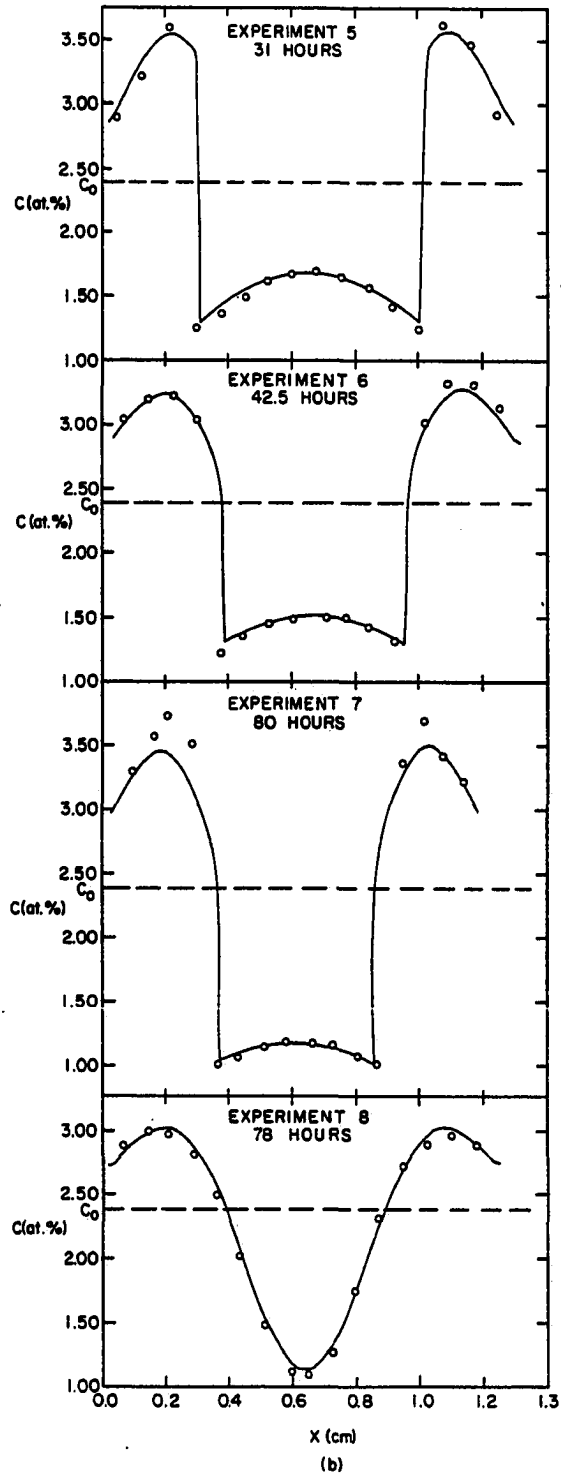
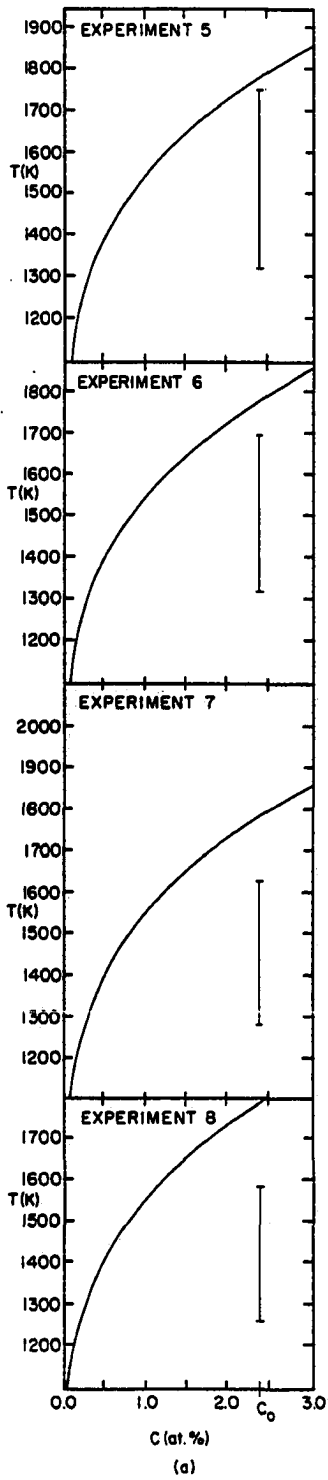
Figure 2. Results of experiments on V-0.457 at.% C alloy showing (a) relative position of temperature range with respect to solvus line, and (b) corresponding concentration profile (o = experimental; — = calculated) for each run



sample of Expt. 1 was in the one-phase condition at the end, as well as at the start of the 22-hour heating period. About 1% and 13% of the samples of Expts. 2 and 3, respectively, were in the two-phase condition initially. At the end of their respective heating times, the sample of Expt. 2 was completely in the one-phase condition, and only a minute fraction of the left end of the sample of Expt. 3 (<1%) was in the two-phase condition. The latter could not be detected experimentally due to the grinding losses on the ends of the sample. Approximately 67% of the sample of Expt. 4 was below the solvus line at the start, as compared to only 30% at the end of a 120 hour run.

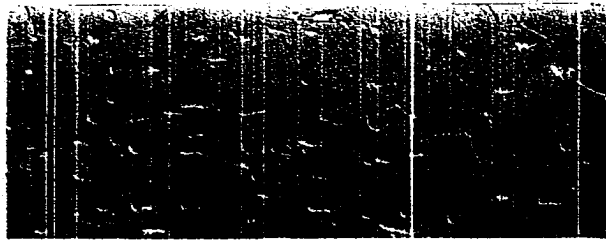
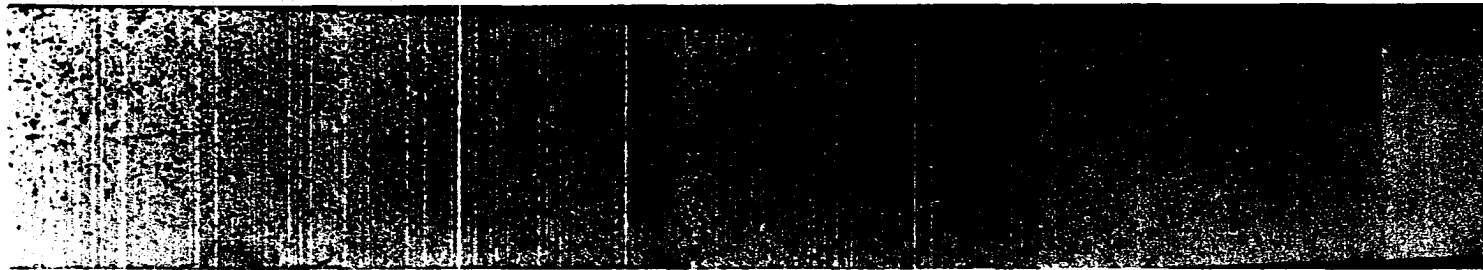
The position of the temperature ranges with respect to the solvus line, and the resulting concentration profiles (both calculated and experimentally determined) are shown in Figure 3 for the experiments on the V-2.388 at.% C alloy (Expts. 5-8). As can be seen from these figures, and Table 5, all of the specimens were in the completely two-phase condition initially, but at the end of their respective heating periods, they were all in the partially two-phase condition with the exception of the sample of Expt. 8. A comparison of the conditions and results of Expts. 6 and 7 indicates that lower temperatures can be compensated for by longer heating times to obtain similar results. On the other hand, the samples of Expts. 7 and 8 were in the partially and completely two-phase conditions, respectively, at the end of similar heating times, indicating that a one-phase region develops earlier in a sample heated at higher temperatures (Expt. 7) than in one at lower temperatures.

Figure 3. Results of experiments on V-2.388 at.% C alloy showing (a) relative position of temperature range with respect to solvus line, and (b) corresponding concentration profile (o = experimental; — = calculated) for each run

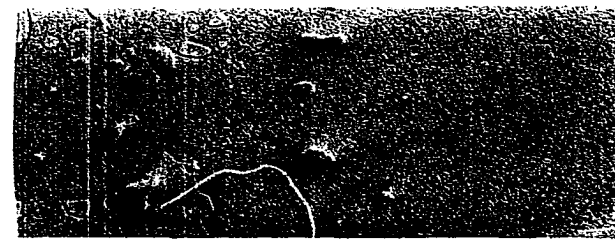


The results presented above and the observations made therein were further supported by the metallographic examination of each sample after the run. Micrographs of the entire left half of the sample from the V-2.388 at.% C alloy (Expt. 7), together with those of higher magnification at various locations, can be seen from Figure 4. They show the presence of the one- and two-phase regions separated by a rather clear boundary. This is consistent with the corresponding concentration profile (Figure 3(b)) in which the pile-up at each end represents the two-phase regions, and the middle region with a maximum at the hottest midpoint represents the carbide-free one-phase region. On the other hand, the fact that the entire specimen of Expt. 8 was in the two-phase condition throughout the run can be seen from Figure 5. It shows that the  $V_2C$  particles were present in the entire specimen, as indicated by the continuous concentration profile with carbon pile-up at the colder regions, and depletion from the hotter middle region of the sample (Figure 3(b)). In Figures 4 and 5, the larger particles with well-defined boundaries are the carbide particles that were present at corresponding temperatures, whereas the finely dispersed ones have formed upon cooling.

The last column in Table 5 shows the values of apparent heats of transport,  $Q_{app}^*$  which were obtained using the data from the one-phase region of each of the samples that were in the partially two-phase condition. It can be seen that  $Q_{app}^*$  values for Expts. 1-3 are close to that of  $Q^*$  for carbon in vanadium,  $-42.3$  kJ/mol [12], inasmuch as these samples were almost entirely in the one-phase condition at the



(a)

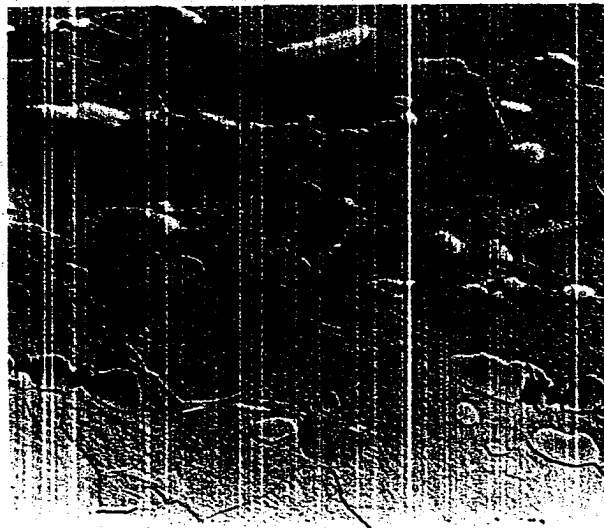
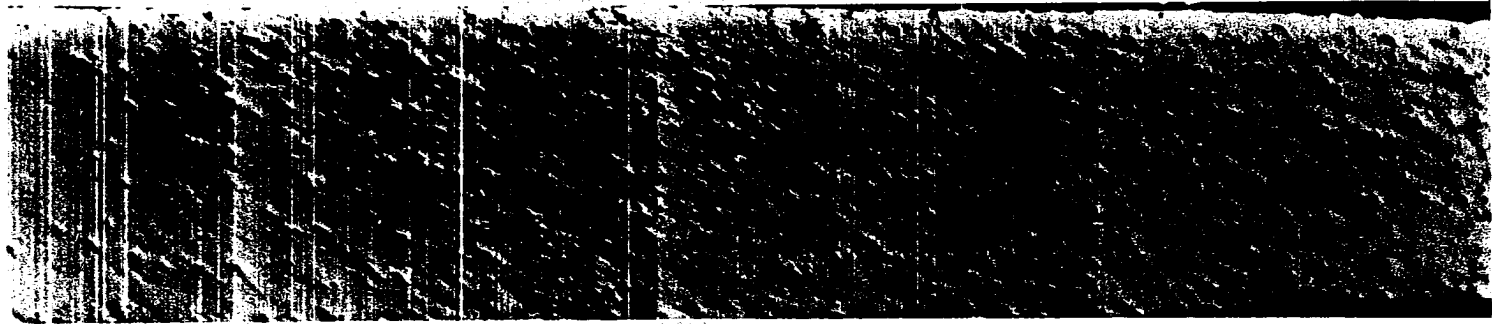


(c)

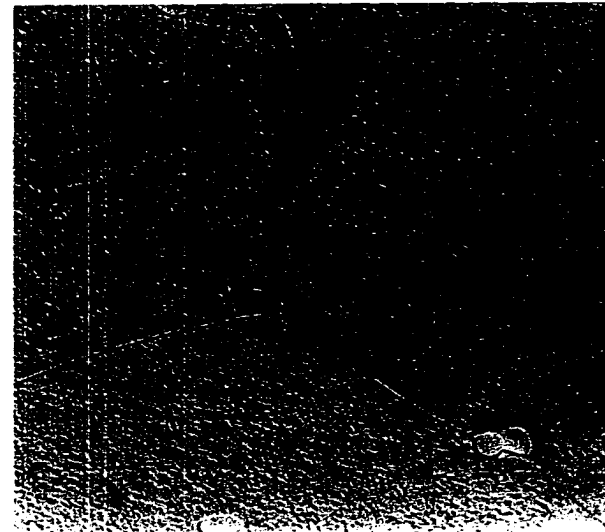


(b)

Figure 4. Optical micrograph of entire half of V-2.388 at.% C sample (Expt. 7) with cold end at left, 36X, BF, and of areas (a) near cold end, (b) midway between hot and cold ends, and (c) at interface between one- and two-phase regions of same sample, 250X, DIC



(a)



(b)

Figure 5. Optical micrograph of entire half of V-2.388 at.% C sample (Expt. 8) with cold end at left, 55X, DIC, and of areas (a) near cold end, and (b) near hot end of same sample, 500X, DIC

conclusion of the heating periods. However,  $Q_{app}^*$  for Expts. 4-7 varied from -50.2 kJ/mol to -64.8 kJ/mol, and hence, are considerably larger in magnitude than  $Q^*$ . This is attributed to the fact that a large fraction of each of these samples was in the two-phase condition at the end of their respective runs. The above trends will be explained in a later section.

#### Carbon Mass Transport in Niobium

The results of the experiments on Nb-C samples (Expts. 10-18), summarized in Table 6, are similar to those obtained from the V-C samples. The initial carbon contents of the samples were 0.347 at.% for Expts. 10-12, and 1.936 at.% for Expts. 13-18.

As is seen from Table 6, the sample of Expt. 10 was virtually all in the one-phase condition at the end of a 96-hour heating period, although 57% of it was in the two-phase condition initially. The samples of Expts. 11 and 12 were heated for 153.5 and 171 hours, respectively, under similar temperature gradients, and both were in the completely two-phase condition initially. However, at the end of their respective heating times, 55% of the former was free of carbides, as compared to 73% of the latter, indicating a displacement of the phase boundary toward the colder regions upon longer heating times.

The positions of the temperature ranges with respect to the solvus line, and the corresponding concentration profiles are shown in Figure 6 for three of the higher carbon samples (Expts. 13, 17, 18).

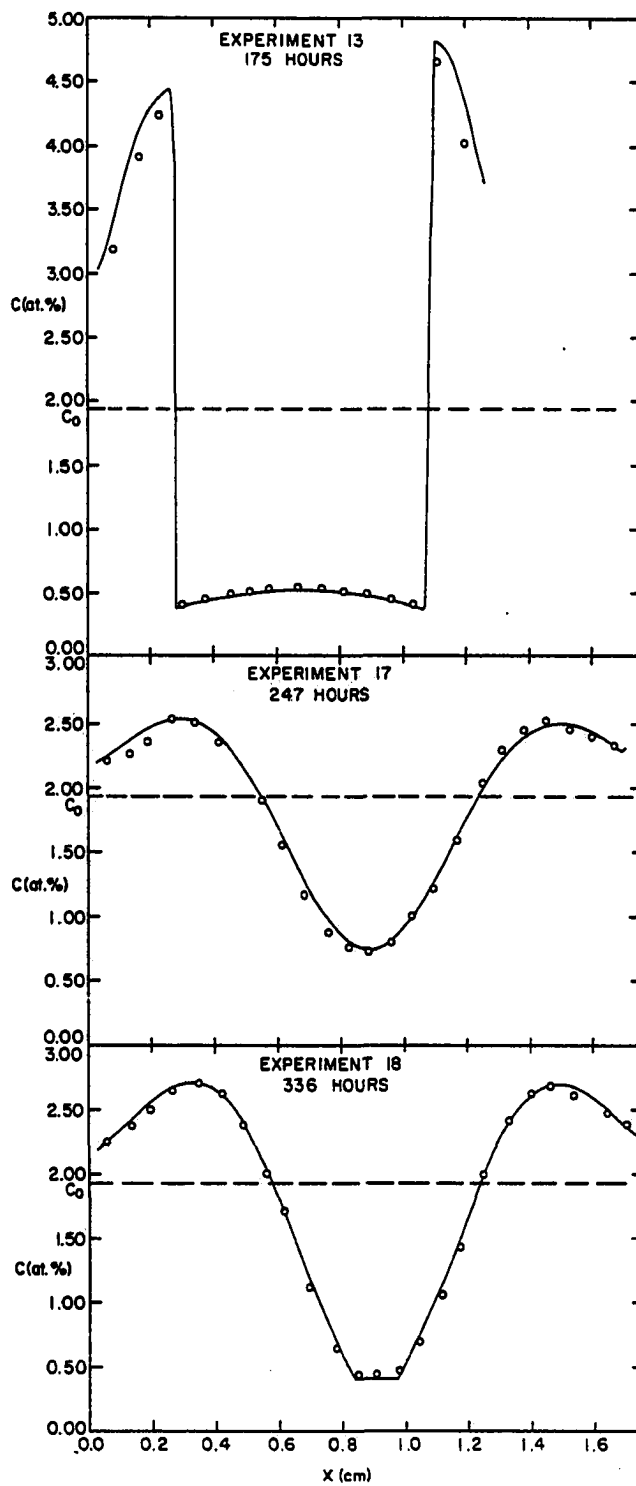
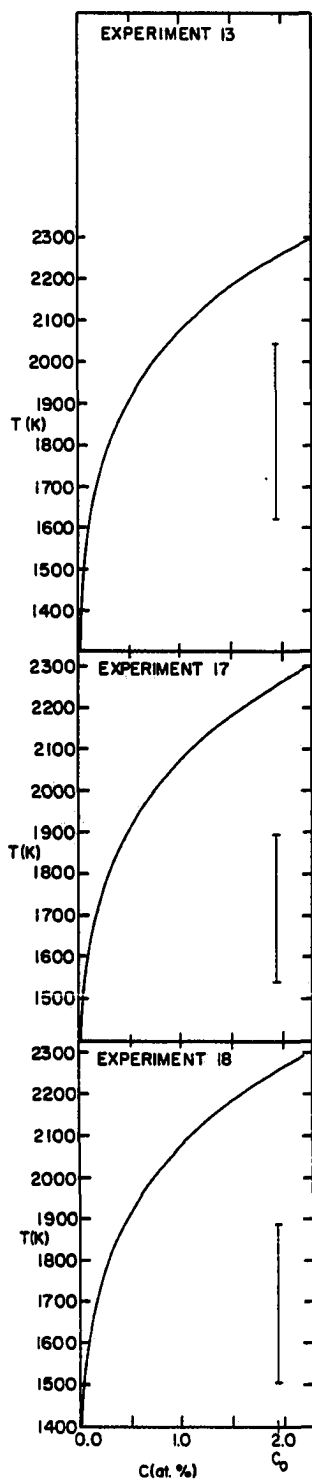
Table 6. Summary of experimental results for mass transport of carbon in niobium under a temperature gradient

Experiment number	Carbon concentration (at.%)	Temperature range (K)			Temperature at solubility limit (K)	Heating period (hours)	% of sample in two-phase condition <sup>a</sup>		Q <sub>app</sub> <sup>* b</sup> (kJ/mol)
		High	Low				Initial	Final	
			Left	Right					
10	0.347	1888	1643	1717	1849	96.0	57	<3	-54.1
11	0.347	1824	1452	1474	1849	153.5	100	45	-71.1
12	0.347	1823	1585	1539	1849	171.0	100	27	-70.2
13	1.936	2043	1624	1654	2260	175.0	100	38	-64.0
14	1.936	1979	1589	1591	2260	82.0	100	100	--
15	1.936	1951	1535	1582	2260	142.0	100	100	--
16	1.936	1936	1649	1630	2260	15.0	100	100	--
17	1.936	1895	1540	1595	2260	247.0	100	100	--
18	1.936	1888	1505	1544	2260	336.0	100	>95	--

<sup>a</sup>Determined from ratio of sample length below temperature of solubility limit for a given carbon concentration to its total length.

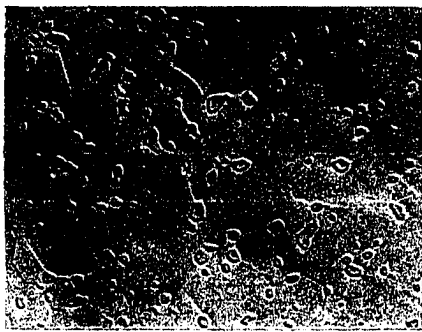
<sup>b</sup>Obtained from slope of a plot of  $\ln C$  versus reciprocal temperature as determined by least squares analysis of data from one-phase regions of partially two-phase samples.

Figure 6. Results of experiments on Nb-1.936 at.% C alloy showing (a) relative position of temperature range with respect to solvus line, and (b) corresponding concentration profile (o = experimental; — = calculated) for each run



As can be seen from these figures and Table 6, the temperature range of Expt. 17 was similar to that of Expt. 18, and its sample was in the completely two-phase condition at the end, as well as at the beginning, of a 247-hour run. The sample of Expt. 18 was also in the completely two-phase condition initially, but a one-phase region has formed at its hotter middle region at the end of a 336-hour heating period, and constituted about 5% of the entire sample. Since the high and the low concentrations in that region varied by less than 1%, it appears as a straight line in both the calculated and experimentally determined profiles. However, the presence of a carbide-free region in the middle portion of the sample of Expt. 18 can be seen from Figure 7, which consists of a series of micrographs of the cross-sectional areas at various locations of the sample. It also illustrates the distribution of the size and amount of the second phase particles along a two-phase Nb-C thermotransport sample.

The value of the apparent heat of transport,  $Q_{app}^*$ , obtained from Expt. 10, i.e., -54.1 kJ/mol, is comparable to  $Q^*$  reported [15] for carbon in niobium, -54.8 kJ/mol; however, the values of  $Q_{app}^*$  obtained from the one-phase regions of the specimens of Expts. 11-13 varied from -64 to -71 kJ/mol, as can be seen from the last column of Table 6, and are larger in magnitude than  $Q^*$ . Observations similar to those described above were made for the V-C samples as mentioned in the previous section.



(a)



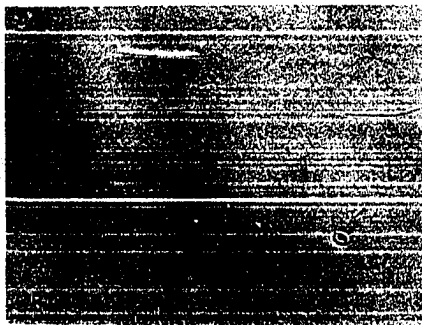
(b)



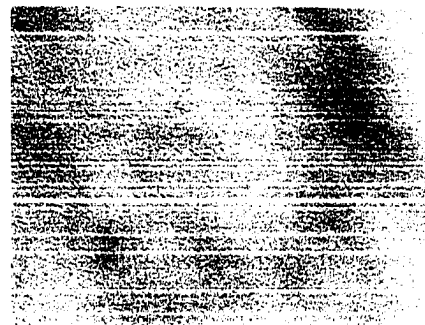
(c)



(d)



(e)



(f)

Figure 7. Optical micrographs showing cross-sectional areas of Nb-1.936 at.% C sample (Expt. 18) that were at (a) 1537 K, (b) 1619 K, (c) 1722 K, (d) 1847 K, (e) 1880 K, and (f) 1886 K during run, 250X, DIC

### Role of Second Phase Particles

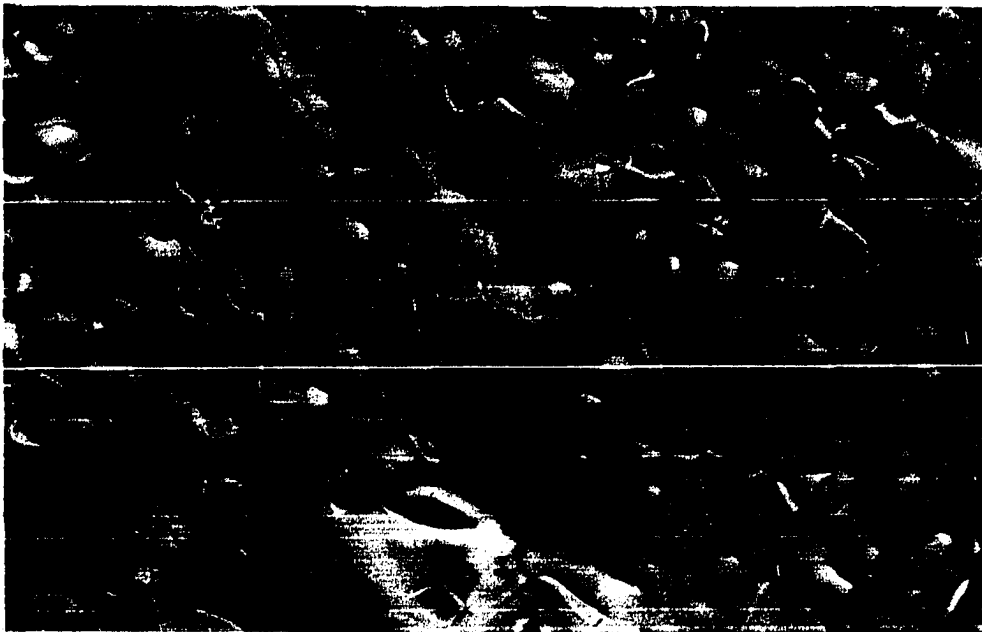
The results of experiments carried out to determine the behavior of second phase particles in mass transport under a temperature gradient can be represented by the micrographs in Figure 8. It shows the same area of a V-2.388 at.% C sample after being heated for 26 hours, and for an additional 5 hours. The sample temperature at the indentation was about 1410 K, and increased from right to left of the indentation.

An examination of the micrographs shows that each particle could be identified before and after the 5-hour heating period. From a comparison of Figure 8(a) with 8(b), the following observations can be made:

- a) Some smaller particles dissolved completely, leaving pits behind.
- b) Most of the particles grew in size and changed shape, and some new particles have formed.
- c) There is no general trend in the direction of growth; for example, the particles encircled at the left of the indentation appear to show more growth on the hotter sides, whereas those to the right of the indentation show more growth on their colder sides.



(a)



(b)

Figure 8. Optical micrographs of same area of V-2.388 at.% C sample after heating (a) 26 hours and (b) an additional 5 hours under same temperature gradient, 400X, DIC

## DISCUSSION OF RESULTS

## The Cross-Sectional Area Effect

As noted earlier, the cross-sectional area factor,  $a_i$ , is unity for one-phase thermotransport, hence its inclusion is of no consequence. Furthermore, its effect is negligible, i.e.  $a_i \sim 1$ , for the two-phase case if the amount of second phase particles is small. However, as the fraction of the cross-sectional area of the sample occupied by the second phase particles increases, the effect of  $a_i$  becomes more pronounced.

The results of an experiment on a Nb-1.936 at.% C alloy (Expt. 13), and the concentration profiles calculated with and without the  $a_i$  factor, using the same conditions, are seen from Figure 9. The profile calculated with the  $a_i$  term shows notably less carbon pile-up at the colder regions than that calculated without it. As can be seen from the figure, the experimental results conform better to the former than to the latter.

The discrepancy between the concentration profiles calculated with and without the  $a_i$  factor would be even greater if the heating time was longer, and/or the initial concentration higher, as can be seen from Figure 10. It shows the profiles calculated for both cases for a V-15.0 at.% C specimen heated for 500 hours under the same parabolic temperature gradient as that of Expt. 6, with the high temperature of 1692 K, and low temperatures of 1334 K at the left and 1315 K at the right end of the sample.

Figure 9. Plots of concentration versus distance showing effect of cross-sectional area factor for Nb-1.936 at.% C sample (Expt. 13)

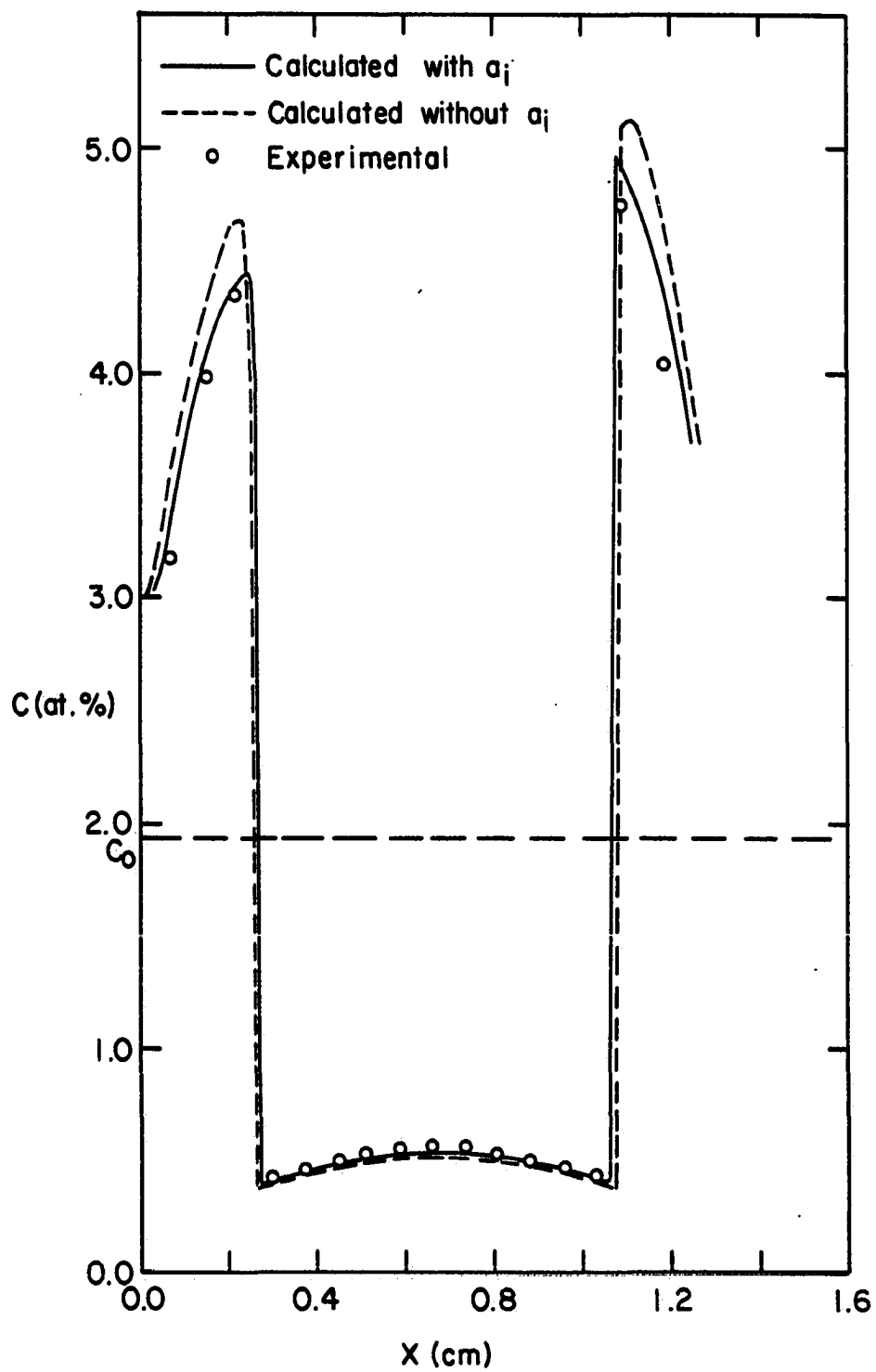
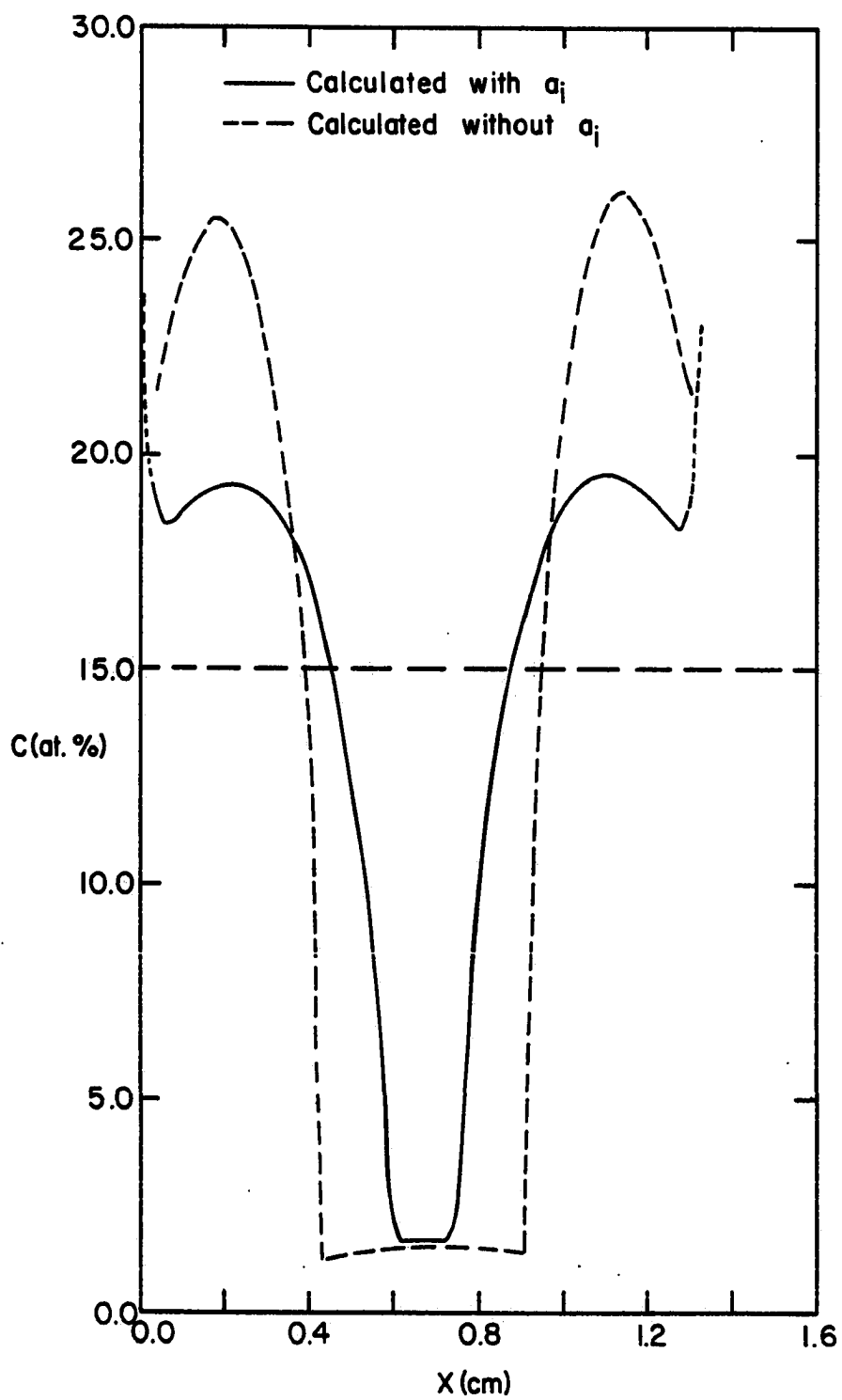


Figure 10. Calculated concentration profiles showing effect of cross-sectional area factor for V-15.0 at.% C specimen heated under a parabolic temperature gradient with  $T_{\text{high}} = 1692$  K and  $T_{\text{low}} = 1334$  K at left and 1315 at right end of sample

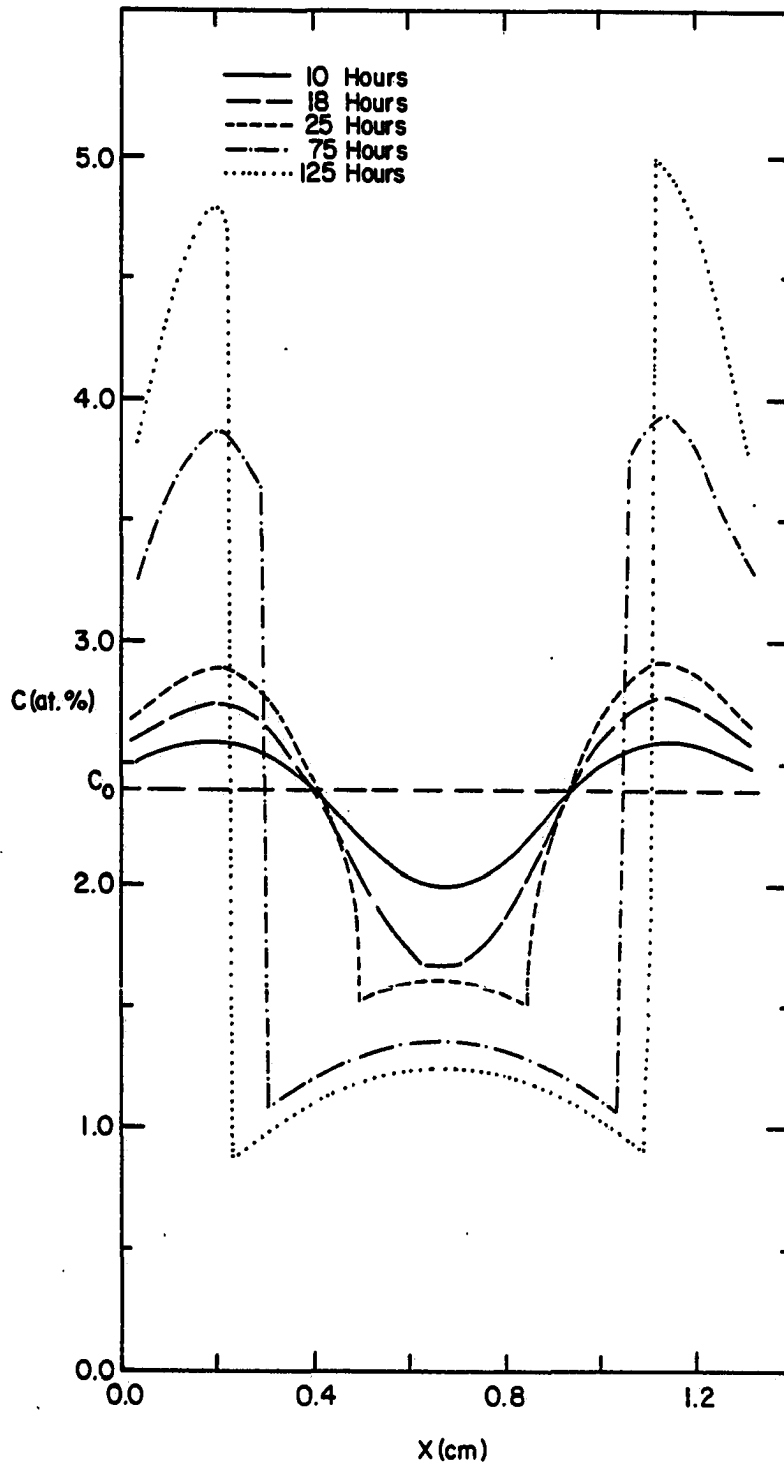


As can be seen from the above discussions, the experimental results agree better with the calculations when the  $a_1$  term is taken into account. This is in accordance with the assumption that diffusivity of the interstitial solute is negligible through the second phase. Furthermore, as a consequence of the cross-sectional area effect, attainment of a steady-state condition in a two-phase alloy, described as "transferring all the solute to one end of the specimen" [4], is virtually impossible, especially when  $Q^*$  and  $\Delta\bar{H}$  have opposite signs.

#### Calculated and Experimental Concentration Profiles

There is excellent agreement between the calculated and experimental results, as can be seen from Figures 2(b) and 3(b) for the experiments on the V-0.457 at.% C and V-2.388 at.% C alloys, respectively, and from Figure 6(b) for those on the Nb-1.936 at.% C alloy. The results give some indication of the physical development of the concentration profiles as a function of time and temperature. However, the mathematical and physical aspects of two-phase mass transport under a temperature gradient can be better understood from an examination of the changes in the concentration profile with time, as can be seen from Figure 11. This figure shows the profiles calculated at 10, 18, 25, 75 and 125 hours for a V-2.388 at.% C specimen. In these calculations, the temperature gradient used was parabolic in shape with the high temperature of 1692 K, and low temperatures of 1334 K and 1315 K at the left and right ends of the sample, respectively. The concentration profiles in Figure 11 are

Figure 11. Calculated concentration profiles for V-2.388 at.% C sample heated under a parabolic temperature gradient ( $T_{\text{high}} = 1692$  K,  $T_{\text{low}} = 1334$  K at left and 1315 K at right end) showing their development with time



representative of those obtained from the experiments on V-C and Nb-C alloys in this study, and will be used as the basis of the following discussions.

The sample used was a two-phase alloy with a uniform distribution of dissolved carbon and  $V_2C$  particles throughout, and it was also in the completely two-phase condition at the start of the heating period. The initial carbon concentration profile of the sample is represented by the Co-line in Figure 11. However, a concentration gradient defined by the solvus line develops for carbon in solid solution upon the application of the temperature gradient, since the solid solubility of carbon in vanadium (also in niobium) decreases with decreasing temperatures. This gives rise to chemical potential differences between the dissolved carbon at high and lower temperatures. Therefore, the driving force due to the partial molar enthalpy of solution for carbon in the metal,  $\Delta\bar{H}$ , arising from the concentration gradient affects the transport behavior of carbon, in addition to that due to the heat of transport,  $Q^*$ . Consequently, the direction and magnitude of net carbon transport in the two-phase sample is dictated by the sign and magnitude of  $(Q^* + \Delta\bar{H})$  in Equation (4). For carbon in vanadium, as well as in niobium,  $\Delta\bar{H}$  is positive, and greater in magnitude than  $Q^*$ , which is negative. In other words,  $(Q^* + \Delta\bar{H})$  is positive, indicating a net transport of carbon toward the colder region of the sample, a reversal in the transport direction from the one-phase thermotransport.

Upon continued heating, the migration of carbon from the hot to colder regions of the sample results in the growth of the particles and/or formation of new ones in the latter region, accompanied by their dissolution in the former. This occurs since concentration of dissolved carbon is fixed by its solubility limit in a particular region, i.e. the carbide particles act as sources and sinks for the dissolved carbon to maintain local equilibrium between carbon in solid solution, and that in the particles. The increase in the amount of carbides, i.e. in the fraction of the cross-sectional area occupied by them, together with the decrease in the mobility of carbon with decreasing temperature, results in the formation of a maximum in the colder region of the sample. This indicates that the rate of carbon migration into the region around the maximum is greater than that out of it. Thus, the concentration profile of the completely two-phase sample is continuous in shape with carbon pile-up in the colder regions, and depletion in the hotter ones, as can be seen from the 10-hour profile in Figure 11.

The migration of carbon from hot to colder regions continues as long as the sample is in the completely two-phase condition. However, upon complete dissolution of the carbide particles, a one-phase region forms in the hottest portion of the sample which expands toward the colder ends with time. The temperature gradient in the vicinity of the temperature maximum is very small. Consequently, the concentration gradient in the region during the earlier stages of its formation is also very small, and appears as almost a straight line, as can be seen from

the 18-hour profile in Figure 11. This was also observed in a Nb-1.936 at.% C sample (Expt. 18), as mentioned in an earlier section.

In the one-phase region, only the thermotransport of carbon toward the hotter region occurs due to negative  $Q^*$ , resulting in the formation of a maximum at the hottest point of the sample. On the other hand, in the two-phase regions, carbon continues to migrate toward the colder ends due to positive  $(Q^* + \Delta\bar{H})$ . Further heating of the sample merely results in more carbon pile-up in the colder (two-phase) regions and in further expansion of the one-phase region, as can be seen from the 25-, 75- and 125-hour profiles in Figure 11.

#### $Q_{app}^*$ Versus $Q^*$

The apparent heat of transport,  $Q_{app}^*$ , is obtained from the one-phase region of a partially two-phase sample, whereas  $Q^*$  is determined from a completely one-phase thermotransport sample at steady state. As was noted earlier, the values of  $Q_{app}^*$  for carbon in both vanadium and niobium are greater in magnitude than the corresponding  $Q^*$  values, which is predicted by the model as can be seen from the following discussion.

As was mentioned earlier, carbon migrates toward the hotter portion in the one-phase region (negative  $Q^*$ ), and toward the colder end in the two-phase region (positive  $(Q^* + \Delta\bar{H})$ ) of a partially two-phase sample under a temperature gradient. In other words, carbon migrates in both directions from the boundary separating the one- and two-phase

regions. This results in a concentration profile in the one-phase region that is steeper than what would have been obtained from a completely one-phase sample, hence, in values of  $Q_{app}^*$  that are larger in magnitude than of  $Q^*$ . However, the motion of the boundary toward the colder end occurs at a decreasing rate, as can be seen from an examination of the 25-, 75- and 125-hour profiles in Figure 11. Therefore, as the sample is heated for longer times, the carbon distribution in the one-phase region should approach that at steady state, i.e. the magnitude of  $Q_{app}^*$  should approach that of  $Q^*$ .

The above interpretation is supported by the values of  $Q_{app}^*$  obtained from the one-phase regions of the different profiles in Figure 11. The results are given in Table 7, together with  $Q_{app}^*$  obtained from 42.5-hour run (Expt. 6), and a 900-hour run (calculated). As can be seen from the table,  $Q_{app}^*$  is 51.0 kJ/mol after only 25 hours, but after a heating period of 900 hours, it is -42.5 kJ/mol, which is close to the value of  $Q^*$  for carbon in vanadium [12], -42.3 kJ/mol as obtained from our one-phase thermotransport experiments.

#### The Role of the Second Phase Particles

In their publication on two-phase mass transport of carbon in Fe-Ni alloys under a temperature gradient, Okafor et al [3] discuss the possibility of changes in the locations of the carbide boundaries by precipitation on the "windward" side, and dissolution from the "leeward" side of a particle at an equal rate. This suggests that an apparent

Table 7. Values of  $Q_{app}^*$  calculated from one-phase region of a V-2.388 at.% C sample heated for various times

Time (hours)	$Q_{app}^*$ (kJ/mol)
25.0	-51.0
42.5	-50.6
75.0	-48.3
125.0	-46.5
900.0	-42.5

motion of carbides would occur "against the solute wind" without any changes in their volumes. Since the net carbon flux in the Fe-Ni alloys, as well as in vanadium and niobium, is toward the colder regions (positive  $(Q^* + \Delta\bar{H})$ ), the apparent particle motion suggested above should be toward the hotter regions of the sample.

The results of the experiments carried out in this study to determine the behavior of the carbide particles in a two-phase V-C sample under a temperature gradient are presented in an earlier section (Figure 8). These results do not show any indication of particle motion, or preferential growth in either the colder or hotter directions. As noted earlier, in any region of a two-phase sample, the amount of carbon in the matrix phase is fixed by its solid solubility limit at the corresponding temperature. Hence, the particles in a

location grow due to an increase in the amount of carbon that is in excess of the solubility limit. These and all the other results obtained in this investigation indicate that the carbide particles act solely as sources and sinks to maintain equilibrium between carbon in solid solution and that in the carbides. This is consistent with the mathematical model used to calculate the concentration profiles in this, and other studies [2-4, 13, 14] on the two-phase mass transport under a temperature gradient in different metal interstitial systems.

#### Solid Solubility of Carbon in Vanadium

In a two-phase V-C (or Nb-C) sample under a temperature gradient, local equilibrium was assumed to exist between carbon in solid solution, and that in the carbide particles. Consequently, there should be a local equilibrium, also, between carbon in the one-phase and two-phase regions of a partially two-phase sample. Therefore, the carbon concentration at the boundary between the one- and two-phase regions should be its solid solubility limit in the metal at the corresponding temperature, as has been reported to be the case for hydrogen in zircaloy [4].

The locations of the boundaries between the one- and two-phase regions were measured precisely from the metallographic examination of the partially two-phase V-C samples. From the corresponding temperature and concentration profiles of each sample, the solubility data, shown in Table 8, were obtained. The heat of solution for carbon in vanadium was determined to be  $86.8 \pm 2.9$  kJ/mol from a least square

analysis of these data. This value is in good agreement with that reported by Ghaneya and Carlson [27],  $83.7 \pm 0.3$  kJ/mol, who used a conventional equilibration method. However, the value reported by Gebhardt et al. [28], 245 kJ/mol, is much higher than either of these values. The results obtained in this study, together with that of Ghaneya and Carlson [27], can be seen from a semilog plot of concentration versus the reciprocal temperature (Figure 12).

Table 8. Solid solubility data for carbon in vanadium obtained from partially two-phase thermotransport experiments

Temperature (K)	Concentration (at.%)
1606	1.1769
1604	1.1990
1614	1.1938
1608	1.1705
1596	1.3159
1604	1.3300
1530	0.9179
1543	0.9782
1300	0.2652
1305	0.2760

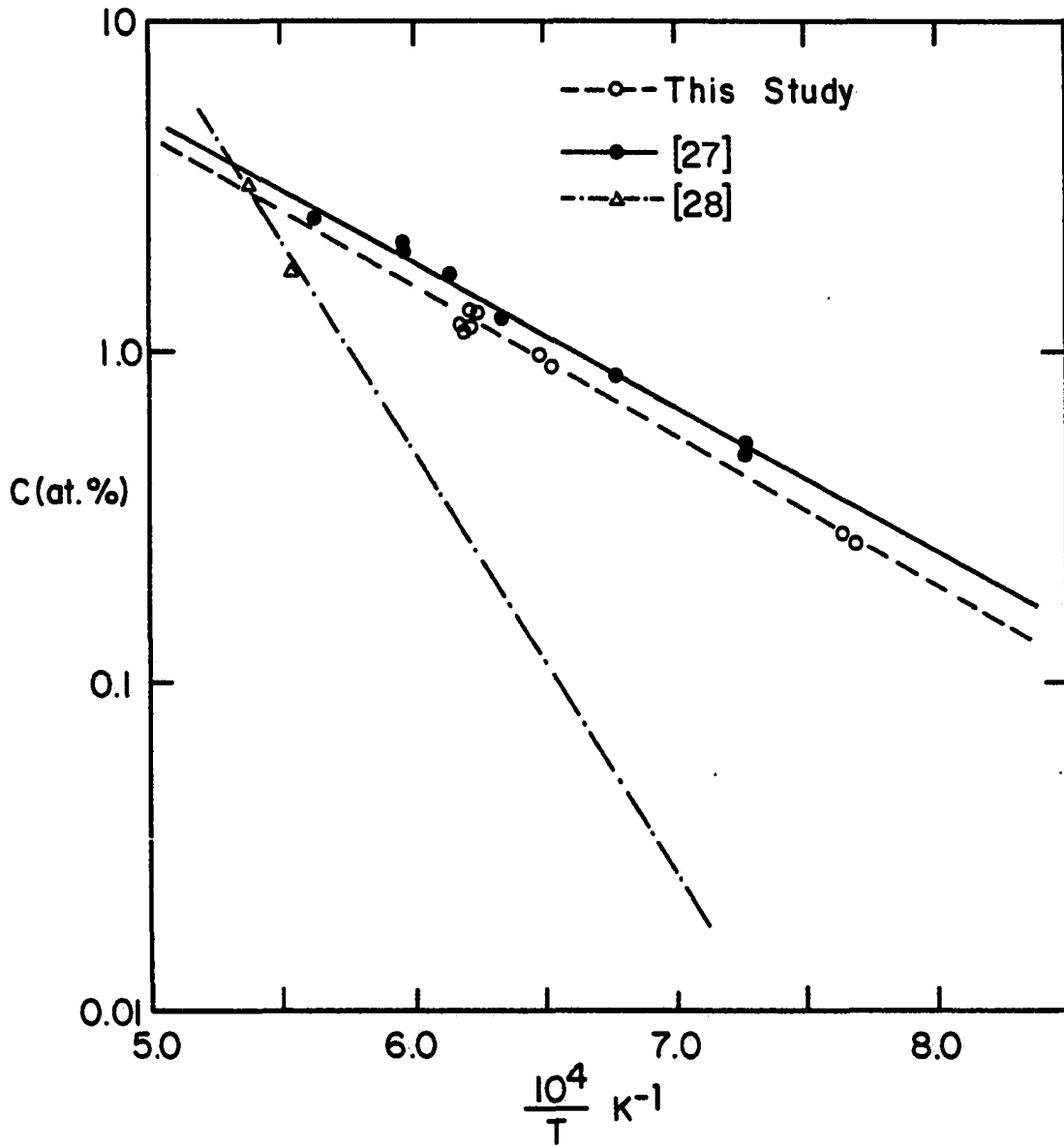


Figure 12. Plots of log concentration versus reciprocal temperature for solid solubility of carbon in vanadium

## CONCLUSIONS

The mass transport of carbon in vanadium and niobium under a temperature gradient was studied in the one-phase, and partially or completely two-phase conditions. The following conclusions were drawn from the results obtained.

1) A mathematical model developed from an irreversible thermodynamics approach was used to correctly predict the experimental results.

- a) Following from the assumption that carbon is transported only through the matrix phase, it is shown that a cross-sectional area factor has to be taken into account, especially when the solute concentration is high, or the heating period is long.
- b) The direction and magnitude of transport are represented by the sign and magnitude of  $Q^*$  in the one-phase region, and by the sign and magnitude of the quantity  $(Q^* + \Delta\bar{H})$  in the two-phase region of a partially two-phase sample under a temperature gradient.
- c) A one-phase region develops in the hotter region of an otherwise completely two-phase Nb-C or V-C transport specimen upon prolonged heating under a temperature gradient.
- d) The magnitude of the apparent heat of transport,  $Q_{app}^*$ , obtained from the one-phase region of a

partially two-phase sample is greater than that of  $Q^*$  obtained from the one-phase experiments at steady state for carbon in both vanadium and niobium. However, as the sample is heated for longer times, the magnitude of  $Q_{app}^*$  approaches that of  $Q^*$ .

2) There is no evidence of an apparent motion of the carbide particles upon heating a two-phase V-C or Nb-C sample under a temperature gradient. They appear to act as sources and sinks for the dissolved carbon to maintain equilibrium between the carbon in solid solution and that in the carbides.

3) It is shown that the solid solubility of an interstitial solute can be determined from studies on partially two-phase mass transport under a temperature gradient. The solid solubility of carbon in vanadium determined in this study,  $\log C(\text{at.}\%) = 2.918 - 4536/T(\text{K})$ , is in good agreement with that obtained by conventional equilibration method.

## REFERENCES CITED

1. T. Hehenkamp, in Electro- and Thermo-transport in Metals and Alloys, edited by R. E. Hummel and H. B. Huntington (AIME, Inc., New York, 1977), p. 68.
2. P. G. Shewmon, *Trans. Met. Soc. AIME* 212, 642 (1958).
3. I. C. I. Okafor, O. N. Carlson and D. M. Martin, *Metall. Trans. A* 13A, 1713 (1982).
4. A. Sawatzky, *J. Nuc. Mater.* 2, No. 4, 321 (1960).
5. J. Diximier, H. Willermoz and R. Roche, in The High Temperature Reactor and Process Applications (The British Nuclear Energy Society, London, 1975), p. 41.1.
6. R. C. Hought and S. M. Grimes, in Neutron Data of Structural Materials for Fast Reactors, edited by K. H. Böckhoff (Pergamon Press, New York, 1979), p. 312.
7. A. Smith, R. McKnight and D. Smith, in Neutron Data of Structural Materials for Fast Reactors, edited by K. H. Böckhoff (Pergamon Press, New York, 1979), p. 374.
8. R. H. Cooper, Jr., in Refractory Alloy Technology for Space Nuclear Power Applications, edited by R. H. Cooper, Jr. and E. E. Hoffman (Technical Information Center, Office of Scientific and Technical Information, USDOE, Oak Ridge, Tennessee, 1984), p. 14.
9. H. Wever, *Z. Metallkd.* 74, 1 (1983).
10. J. Mathuni, R. Kirchheim and E. Fromm, *Acta Metall.* 27, 1665 (1979).
11. D. T. Peterson and M. F. Smith, *Metall. Trans. A* 13A, 821 (1982).
12. M. Uz and O. N. Carlson, Department of Materials Science and Engineering, Iowa State University, and Ames Laboratory, Ames, Iowa, 1984 (Section I in this thesis).
13. A. Sawatzky and E. Vogt, *Trans. Met. Soc. AIME* 227, 917 (1963).
14. G. P. Marino, *Nucl. Sci. Eng.* 49, 93 (1972).
15. O. N. Carlson, F. A. Schmidt and M. Uz, *J. Less-Common Metals* 79, 97 (1981).

16. S. R. DeGroot, Thermodynamics of Irreversible Processes (Interscience Publishers, New York, 1952).
17. I. Prigogine, Introduction to Thermodynamics of Irreversible Processes, 2nd edition (Interscience Publishers, New York, 1961).
18. K. G. Denbigh, The Thermodynamics of Steady State (John Wiley and Sons, Inc., New York, 1965).
19. F. A. Schmidt and O. N. Carlson, *J. Less-Common Metals* 26, 247 (1972).
20. B. B. Yu and R. F. Davis, *J. Phys. Chem. Solids* 42, 83 (1981).
21. F. A. Schmidt and J. C. Warner, *J. Less-Common Metals* 26, 325 (1972).
22. D. T. Peterson, R. G. Clark and W. A. Stensland, *J. Less-Common Metals* 30, 169 (1973).
23. J. C. Warner, Databook JCW-1, Department of Materials Science and Engineering, Iowa State University, and Ames Laboratory, Ames, Iowa (unpublished data, 1964), p. 10.
24. E. Fromm, *J. Less-Common Metals* 14, 113 (1968).
25. Selected Values of the Thermodynamic Properties of Binary Alloys, prepared by R. Hultgren, P. D. Desai, D. T. Hawkins, M. Gleiser and K. K. Kelley (American Society for Metals, Metals Park, Ohio, 1973), p. 502.
26. E. Rudy, St. Windisch and C. E. Brukl, *Planseeber. Pulvermetall.* 16, 3 (1968).
27. A. Ghaneya and O. N. Carlson, Department of Materials Science and Engineering, Iowa State University, and Ames Laboratory, Ames, Iowa (private communication, 1983).
28. E. Gebhardt, E. Fromm and U. Roy, *Z. Metallkd.* 57, 682 (1966).

## APPENDIX

The concentration profiles resulting from the thermotransport of carbon in one- and two-phase vanadium-carbon and niobium-carbon alloys were calculated using an explicit, single step finite difference method as discussed in the text. Equation (3), the governing equation for the thermotransport of an interstitial solute  $i$  in metals used in these calculations, is reproduced as

$$J_i = - D_i a_i \left[ \frac{dC_i}{dX} + \frac{Q_i^* C_i}{RT^2} \frac{dT}{dX} \right] . \quad (\text{A.1})$$

The assumptions made in the derivation of Equation (A.1), its application to one- and two-phase thermotransport, and the information necessary for the calculation of all its parameters are discussed in pages 60-63. Hence, this section will deal primarily with the procedure used in calculating the concentration profiles.

During the calculations, the sample is treated as consisting of  $n$  segments of equal thickness, with  $N = n + 1$  boundaries, or nodes, which in the present study were 99 and 100, respectively. The thickness of the segments varied from  $1.2 \times 10^{-4}$  m to  $1.8 \times 10^{-4}$  m for different runs, depending on the sample length.

The initial solute concentration distribution throughout the sample is uniform, that is  $\bar{C}_1 = \bar{C}_2 = \bar{C}_3 = \dots = \bar{C}_n$ , where  $\bar{C}_1$  is the overall average solute concentration of segment 1, etc. The solute gradient within a segment is taken to be linear due to its very small thickness.

The temperature profile can be determined from the experimental temperature-position data. In the present study, it is defined by a cubic equation as can be seen from Equation (6) and Figure 1, and the temperature, hence its gradient, at an exact location can be calculated. Then, the fluxes through the nodes on either side of a segment can be calculated using Equation (A.1), and the change in solute concentration of the segment, thus the concentration profile of the entire sample can be determined.

The concentrations,  $\bar{C}_n$  and  $\bar{C}_{n-1}$ , of the two segments  $n$  and  $n-1$  on either side of a node  $I$  are compared to the solubility limit of the interstitial solute,  $C_n(\text{sol})$  and  $C_{n-1}(\text{sol})$ , at corresponding temperatures to determine the conditions (one-phase, two-phase) of the segments, hence of the node. Since the fluxes through the ends of the sample are taken to be zero, all the nodes, except  $I = 1$  and  $I = N$ , are examined. Four possible cases of the conditions of the two adjacent segments and of the node between them are analyzed below.

(a) If  $\bar{C}_n < C_n(\text{sol})$  and  $\bar{C}_{n-1} < C_{n-1}(\text{sol})$ , both segments  $n$  and  $n-1$ , as well as the node between them, are in the one-phase condition. Then, the cross-sectional area factor at node  $I$  is unity, that is

$$a_I = 1 . \quad (\text{A.2})$$

Furthermore, the solute concentration at node  $I$  is defined as

$$C_I = \frac{\bar{C}_n + \bar{C}_{n-1}}{2} , \quad (\text{A.3})$$

and its gradient is

$$\frac{dC_I}{dX} = \frac{\bar{C}_n - \bar{C}_{n-1}}{\Delta X}, \quad (\text{A.4})$$

where  $\Delta X$  is the distance between the midpoints of the two adjacent segments  $n$  and  $n-1$ , or the segment thickness. Then, the fluxes through nodes  $I$  and  $I + 1$ ,  $J_I$  and  $J_{I+1}$  can be calculated using Equation (A.1), and the change in the solute concentration of the segment  $n$ , after heating of the sample for an incremental period of time,  $\tau$ , can be determined from

$$\Delta C_n = \left( \frac{J_I - J_{I+1}}{\Delta X} \right) \tau. \quad (\text{A.5})$$

Finally, the overall average solute concentration of the segment after time  $\tau$ , becomes

$$\bar{C}_n(\tau) = \bar{C}_n + \Delta C_n. \quad (\text{A.6})$$

(b) If segments  $n-1$  and  $n$  are in the one- and two-phase conditions, respectively, then node  $I$  is assumed to be in the two-phase condition<sup>1</sup>, and  $a_I$  is determined from the lever rule as

---

<sup>1</sup>An assumption that node  $I$  is in the one-phase is equally valid, and calculations using either assumption yielded the same results in the present study. One can, however, determine the exact location of the boundary between the one- and two-phase regions by dividing the sample into much smaller segments.

$$a_I = [C_I(\text{carb}) - \bar{C}_I] / [C_I(\text{carb}) - C_I(\text{sol})] . \quad (\text{A.7})$$

In Equation (A.7),  $C_I(\text{carb})$  and  $C_I(\text{sol})$  are the carbide and matrix solubility limit concentrations at the temperature corresponding to node I. Since only the solute in the matrix is assumed to be mobile, it then follows that

$$C_n = C_n(\text{sol}) \text{ and } C_{n-1} = \bar{C}_{n-1} . \quad (\text{A.8})$$

Hence,

$$C_I = \frac{C_n(\text{sol}) + \bar{C}_{n-1}}{2} \quad (\text{A.9})$$

and

$$\frac{dC_I}{dX} = \frac{\bar{C}_{n-1} - C_n(\text{sol})}{\Delta X} . \quad (\text{A.10})$$

Again,  $\Delta C_n$  and  $\bar{C}_n(\tau)$  are calculated using Equations (A.5) and (A.6), respectively.

(c) For the case where segments  $n-1$  and  $n$  are in the two- and one-phase conditions, respectively, node I is in the two-phase condition,  $a_I$  is defined by Equation (A.7), and

$$C_n = \bar{C}_n \text{ and } C_{n-1} = C_{n-1}(\text{sol}) . \quad (\text{A.11})$$

Hence,

$$C_I = \frac{\bar{C}_n + C_{n-1}(\text{sol})}{2} \quad (\text{A.12})$$

and

$$\frac{dC_I}{dX} = \frac{C_{n-1}(\text{sol}) - \bar{C}_n}{\Delta X} \quad (\text{A.13})$$

As for cases in (a) and (b),  $\Delta C_n$  and  $\bar{C}_n(\tau)$  are calculated from Equations (A.5) and (A.6), respectively.

(d) When segments  $n$  and  $n-1$  are both in the two-phase condition, node  $I$  is also in the two-phase condition. In this case,  $a_I$  is again determined using Equation (A.7), and

$$C_I = C_I(\text{sol}) \quad (\text{A.14})$$

Then,

$$\frac{dC_I}{dX} = \frac{dC_I(\text{sol})}{dX} \quad (\text{A.15})$$

and  $\Delta C_n$  and  $\bar{C}_n(\tau)$  are calculated from Equations (A.5) and (A.6).

The flow diagram illustrating the calculations described in the preceding paragraphs can be seen from Figure A.1.

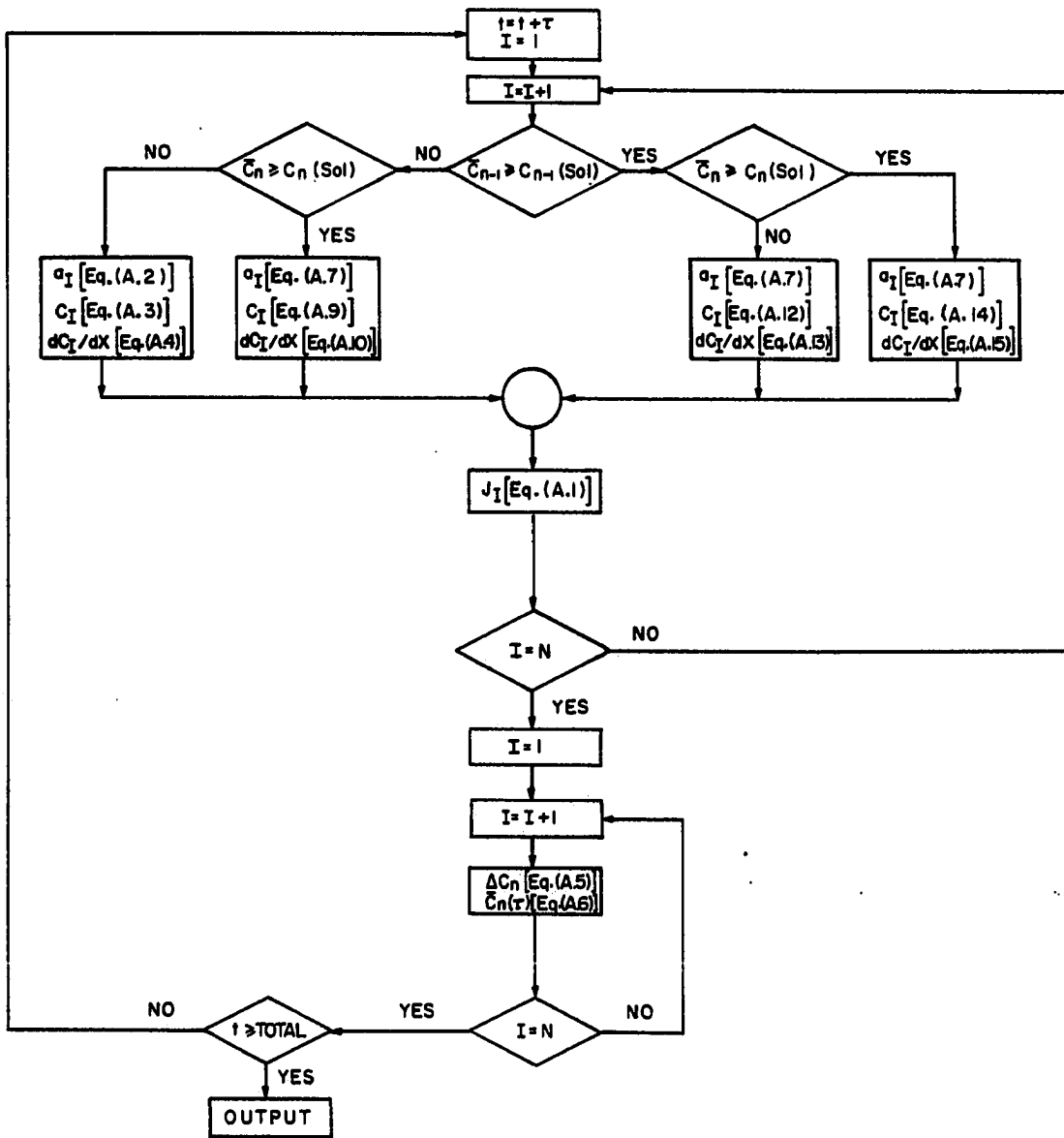


Figure A.1. Flow diagram for the calculation of concentration profiles resulting from the thermotransport of an interstitial solute in metals

## ACKNOWLEDGMENTS

I wish to express my deep gratitude to Professor O. N. Carlson for his knowledgeable and patient guidance, and critical analysis during the course of this research and in the preparation of this manuscript. Special thanks are due Mr. D. K. Rehbein for writing the computer program, Mr. F. A. Schmidt for providing the vanadium and titanium metals, and Mr. H. H. Baker for his superb metallographic work. Thanks are extended to Messrs. M. E. Thompson, L. K. Reed, A. D. Johnson and L. P. Lincoln for their technical assistance, and to R. Z. Bachman and N. M. Beymer for their analytical work. Finally, I would like to thank my wife, Sultan, and my daughter, Emel, for their unselfish devotion, and untiring patience and encouragement during my doctoral studies.